PERGAMON

International Journal of Rock Mechanics and Mining Sciences 36 (1999) 191–215

International Journal of
Rock Mechanics
and Mining Sciences

Drilling-induced tensile wall-fractures: implications for determination of *in-situ* stress orientation and magnitude

M. Brudy[a,*], M. D. Zoback[b]

[a]*Geophysical Institute, University of Karlsruhe, 76187 Karlsruhe, Germany*
[b]*Department of Geophysics, Stanford University, Stanford, CA 93405, USA*

Accepted 30 November 1998

Abstract

Detailed investigation of failure of the borehole wall in two scientific drilling projects, the German KTB (Kontinentales Tiefbohrprogramm der Bundesrepublik Deutschland) and the European geothermal research project at Soultz-sous-Forêts, France, has lead to new insight in the phenomena of tensile fractures induced in the wellbore wall during drilling. Comparison of the orientation of the fractures with the orientation of the horizontal principal stress known from breakout and hydraulic fracturing analysis demonstrates that these fractures are reliable indicators of the orientation of the maximum horizontal principal stress S_H. A model for the initiation of the fractures is presented which points out the important influences of (a) the tectonic stress state, (b) increased mud pressures during drilling operation and (c) thermal stresses induced by circulation of relatively cold drilling mud. Analysis of drilling-induced fractures in the GPK1 borehole at Soultz-sous-Forêts (where the magnitude of S_H is known from hydraulic fracturing experiments) demonstrates the validity of this model for the initiation of the fractures. Further, a new method is proposed to estimate the magnitude of S_H from the occurrence of drilling-induced fractures and knowledge of thermally induced stress and pumping pressure during drilling. The method is successfully applied to both KTB boreholes. An independent method to estimate the magnitude of S_H based on the analytical calculation of the stress intensity factor for drilling-induced fractures taking into consideration both, increased mud pressure and thermal stress, is also presented. Application of this method confirms the results derived with the analysis described above. Additionally, the evaluation of the orientation of the fractures with respect to the wellbore axis indicates that over major depth sections of the investigated wells the vertical stress is a principal stress.

1. Introduction

Drilling-induced compressive and tensile failure of wellbores is a well known phenomenon in hydrocarbon industry. Compressive failure leads to oriented enlargements of the borehole cross-section known as wellbore breakouts [1,2]. Unintensional hydraulic fracturing induced by too high mud pressures is known to cause loss of circulation in wells [3,4]. The orientation of wellbore failures can be determined with geophysical logging tools such as the Borehole Televiewer (BHTV) [5] or Formation MicroScanner/Formation MicroImager[1] (FMS/FMI) tools [6].

In this paper we focus on a type of wellbore failure, drilling-induced tensile wall-fractures, revealed by detailed FMS/FMI logging in two scientific drilling projects, the German KTB (Kontinentales Tiefbohrprogramm der Bundesrepublik Deutschland) and the European geothermal research project at Soultz-sous-Forêts, France. A phenomenological description of this failure type and an analysis for the purpose of the determination of the state of stress is provided. These fractures are observed in pairs, mostly parallel to the nearly vertical wellbore axes and on diametrically opposed sides of the borehole walls. Fig. 1

* Corresponding author. Present address: Statoil Research Centre, Arkitekt Ebbells veg 10, Rotvoll, 7005 Trondheim, Norway. Tel.: +47-73-58-4569; fax: +47-73-96-7286; *E-mail address*: mabr@statoil.no (M. Brudy).

[1] Formation MicroScanner and Formation MicroImager are Trademarks of Schlumberger.

0148-9062/99/$ - see front matter
PII: S0148-9062(98)00182-X

shows two examples of such fractures recorded with the Formation MicroScanner (FMS) and the Formation MicroImager (FMI) in the KTB pilot hole (Fig. 1a) and in the GPK1 borehole at Soultz-sous-Forêts (Fig. 1b), respectively. The fractures are seen as near vertical stripes of reddish colors, indicating high electrical conductivity presumably because drilling mud invaded the fractures. In this paper we will thoroughly describe the phenomenology of the fractures and try to explain their initiation, their orientation, occurrence with depth and trace at the wellbore wall. We will also give an explanation for the initiation

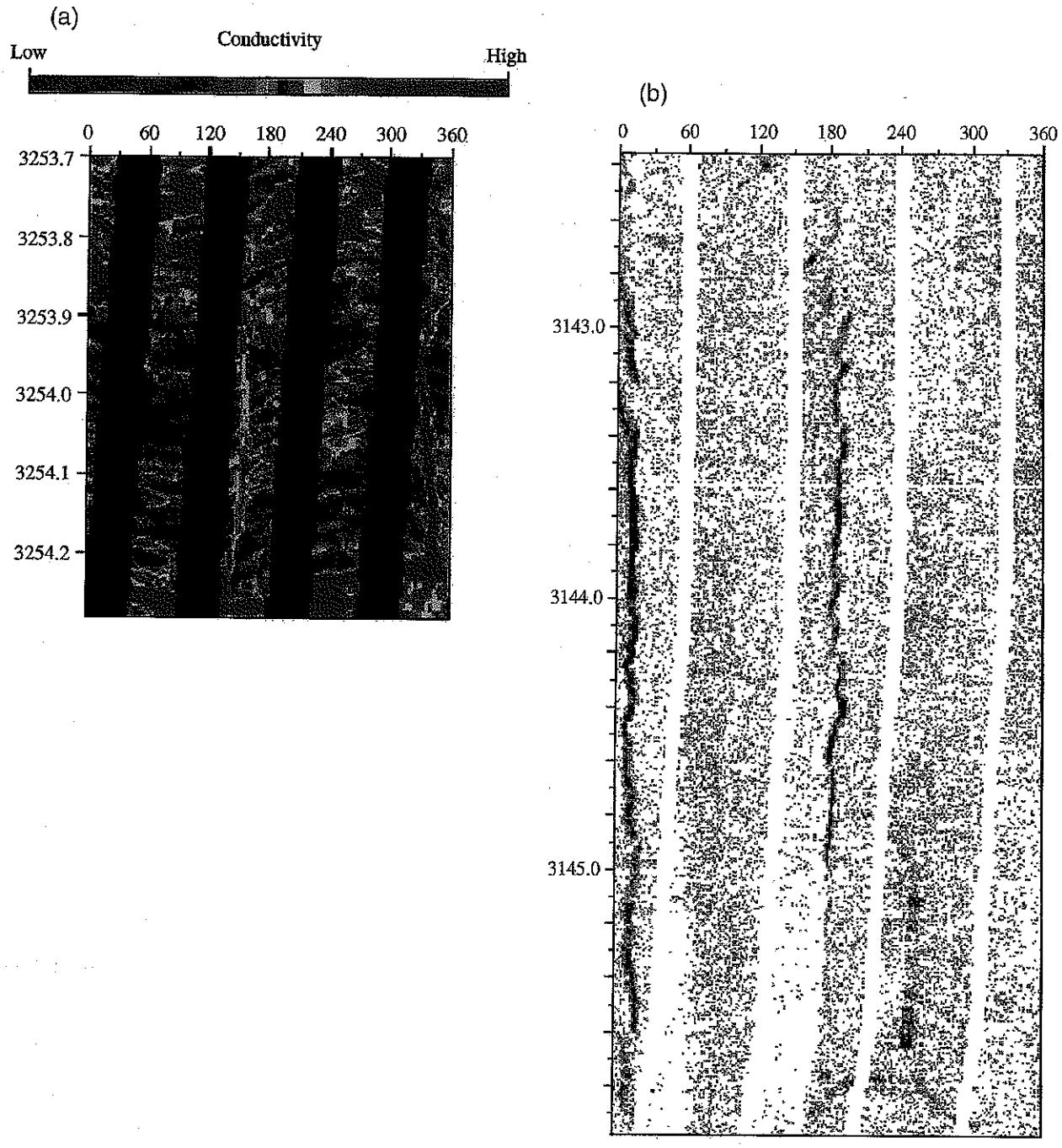

Fig. 1. A Formation MicroScanner image from (a) the KTB pilot hole (depth 3254 m) displays a drilling-induced vertical tensile wall-fracture (near vertical reddish stripes at 170° and 350°) which crosscuts the natural planar structures of the rock (sinusoidal features in reddish colors). Fracture planes are displayed as zones of high electrical conductivity as they are either filled by drilling mud, pore fluid or mineral fillings which all have higher electrical conductivity than the undisturbed rock. (b) An example of a vertical tensile wall-fracture in homogeneous isotropic granite encountered in the GPK1 borehole at Soultz-sous-Forêts is displayed as near vertical dark grey stripes at 20° and 200°. The fracture extends over a depth range of about 3 m.

of the fractures analyzing the various stresses acting on the borehole wall during drilling operation and finally show how the occurrence of these fractures can be used for the estimation of the magnitude of the greatest horizontal principal stress S_H under the precondition that the least horizontal principal stress S_h is known from another method like hydraulic fracturing (e.g. Refs. [7, 8]).

The KTB project [9] was conducted in two phases. Starting in September 1987, a 4000 m deep pilot hole was drilled close to the village of Windischeschenbach in Bavaria, Germany. The KTB main hole, started in October 1990, reached a final depth of 9101 m in October 1994. Both wells were drilled through steeply dipping gneisses and amphibolites, the main hole encountering several major zones of faulting, which were detected seismically [10, 11] and by borehole measurements and also in the cores and cuttings [12–14]. An extensive logging program provided a complete data set of physical, lithological, chemical and technical parameters to a depth of ~8700 m. The KTB pilot hole provided also an almost complete set of cores to a depth of 4 km. Due to the use of a motor steering system to a depth of about 7600 m in the KTB main hole the deviation was kept below 1° to this depth, but increased to about 20° at great depth.

The borehole at Soultz-sous-Forêts [15] is situated in the western part of the Rhine Graben, a rift system extending about 300 km from Basel to Mainz and belonging to the Mid-European Rift System. The location is close to the center of a pronounced geothermal anomaly situated in the Rhine Graben. The geothermal gradient in the Soultz-sous-Forêts area is about 3 times higher than the worldwide average gradient of 30°C/km. The Granitic Soultz Horst is covered by about 1400 m of sediment. Faults trending approximately N–S characterize the tectonic structures of the area. The well was drilled into the basement consisting of relatively homogenous porphyritic granite to a depth of 3590 m.

2. Detection and phenomenology of drilling-induced tensile fractures

Formation MicroScanner (FMS), Formation MicroImager (FMI) and in the case of the KTB main hole also High Temperature Formation MicroScanner (HFMS) were used to gain a picture of natural faults, fractures and foliation of the rock crosscut by the borehole. All three instruments are based on the same physical principal [6]. Small, circular electrodes (diameter ~4 mm) located on four extendible arms which are hydraulically pressed at the wellbore wall emit an electrical current into the rock. The voltage of the electrodes is kept constant and the emitted current is recorded. The magnitude of the current is mainly determined by the resistivity of the rock just in front of the electrode and therefore allows production of a detailed image of the resistivity of the borehole wall. The sampling rate per depth of these tools is in the mm range so that even very thin structures can be detected. Image enhancement routines [16] are used to create images representing contrasts of the resistivity of the wellbore wall. Using an interactive program [16] the images can be displayed and dip angle, dip azimuth and depth of planar structures which are represented by sinusoidal curves can be recorded. The FMI has additionally attached to each arm a mechanical flap, which doubles the width of the electrode arrangement on each arm and, therefore, allows reaching a sufficient coverage of the borehole wall in large bitsize holes. The HFMS has the same configuration of electrodes as the FMS but is especially equipped for withstanding high temperatures and pressure to allow its use in very deep or very hot wells.

Fractures and faults usually differ significantly in their electrical resistivity from the surrounding rock due to water or mud in open fractures or due to mineral fillings with low resistivity (calcite, graphite). Therefore, these tools are ideal for the detection of fractures, faults and foliation planes crosscutting the borehole.

Analyzing the FMS/FMI images for the occurrence of faults and fractures yielded three different types of structures. (1) Sinusoidal structures clearly visible all around the borehole wall. These are the traces of plane faults or foliation planes intersecting the borehole (Fig. 1a). (2) Pairs of traces parallel to the borehole axis offset by 180° and not interconnected around the wellbore wall (Fig. 1) which we call 'drilling-induced tensile wall-fractures' because they are initiated during the drilling process as pure tensile fractures but do not appear to propagate significantly into the rock surrounding the borehole (like a drilling-induced hydraulic fracture) and are thus limited to the borehole wall (this is discussed in detail below). (3) Fracture traces 180° offset at the borehole wall, but inclined with respect to the borehole axis (Fig. 2). This type we call 'en-echelon' fractures as their geometry looks very similar to en-echelon fractures well-known from geology. The origin of these traces is often difficult to determine. In many cases we think they are drilling-induced tensile wall-fractures that are inclined to the wellbore axis due to the fact that none of the principal stress axes is being parallel to the borehole axis [17]. Drilling-induced tensile fractures occurring under these conditions are also discussed in detail below.

Unfortunately, FMS/FMI data quality is sometimes poor because one or two of the arms are not in good contact with the borehole wall or because the borehole

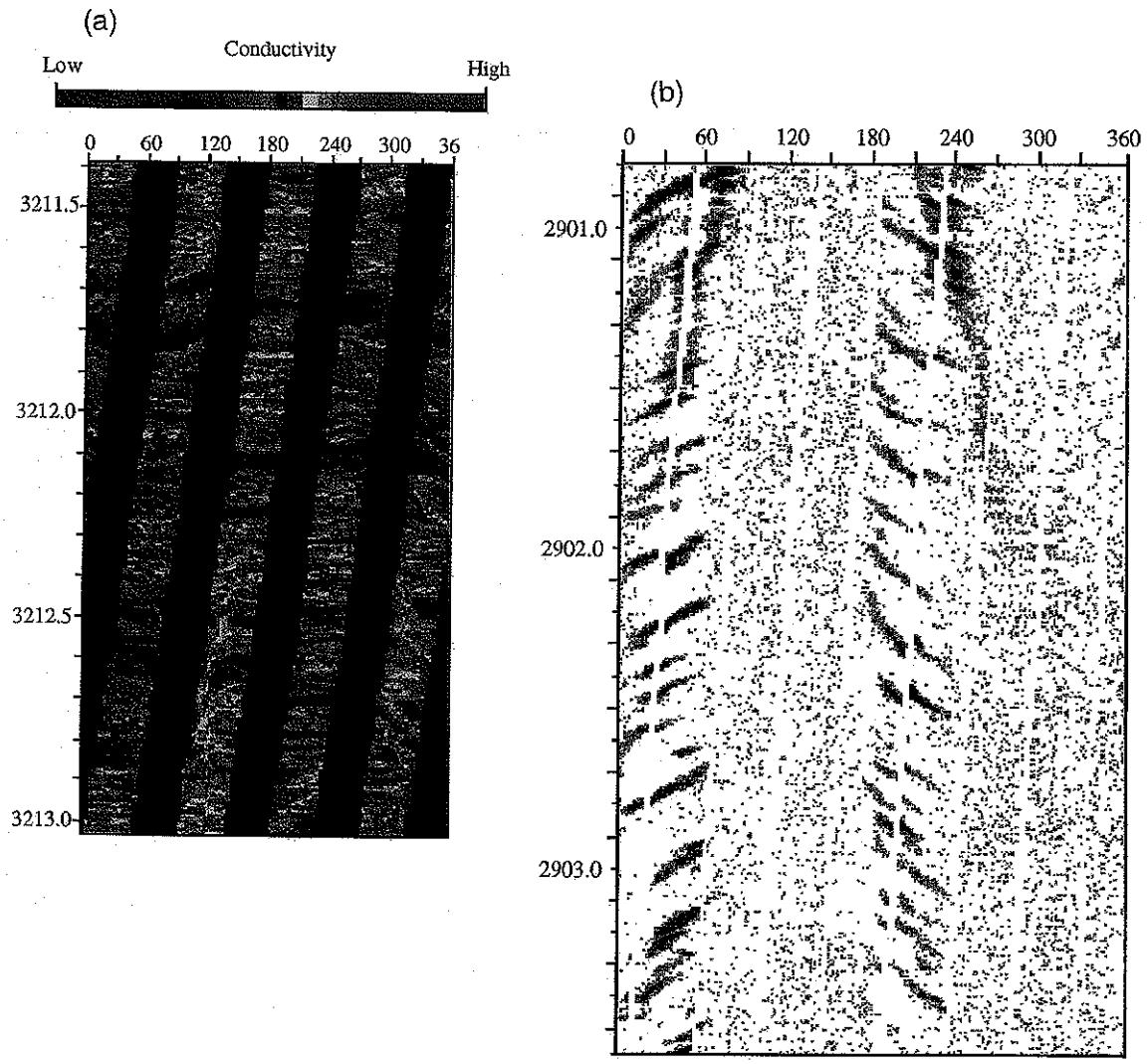

Fig. 2. Rarely also drilling-induced fractures are seen which are inclined to the wellbore axis. The occurrence of this type of fractures is limited to narrow depth sections mostly close to natural faults cross-cutting the borehole. The examples presented here are found (a) in FMS recordings from 3213 m depth from the KTB pilot hole and (b) also in the granites drilled at Soultz-sous-Forêts.

wall is very rough. If a plane fault is intersected by the well in a section with poor data quality its sinusoidal trace may not be fully depicted making it hard to distinguish from en-echelon drilling-induced fractures. Despite such problems, several sections of the KTB pilot hole and the GPK1 well were found where image quality is very good and where the en-echelon fractures are seen clearly drilling-induced. In the GPK1 well such fractures were fairly easy to observe in the relatively homogeneous granites. It is also advantageous that the measurements in the GPK1 well cover about 95% of the borehole wall. Importantly, in the KTB boreholes, in depths where the drilling-induced tensile wall-fractures were detected by FMS/FMI logging no corresponding fractures were observed in the cores [18]. This indicates that the fractures seen in the logging are not natural, preexisting fractures crosscutting the borehole, but instead are fractures initiated in the borehole wall while drilling. It is also important to note that there was never any indication of lost circulation or drilling mud at the depths these fractures were encountered, thus distinguishing them from drilling-induced hydraulic fractures.

Therefore, the following characteristics of drilling-induced tensile fractures are: (1) they occur in pairs on opposite sides of the borehole wall. (2) They can be grouped in two types one trending about parallel to the borehole axis and the others occurring at an angle to the borehole axis (en-echelon type). (3) Their length ranges commonly between 0.1 and 2.0 m. (4) They clearly occur in the KTB boreholes at the azimuth of the greatest horizontal principal stress S_H [19] where the tangential stresses are least compressive (see below). (5) Usually the traces of the fractures show small kinks and are not perfectly straight.

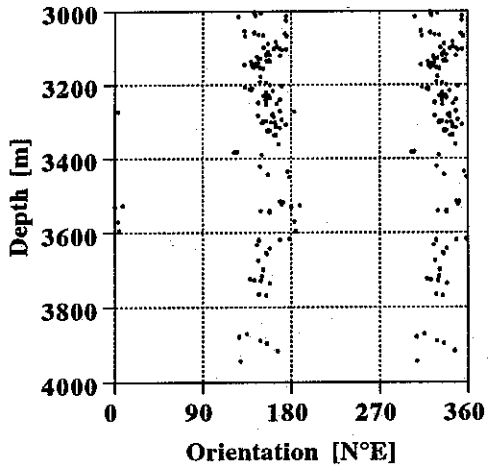

Fig. 3. FMS measurements in the KTB pilot hole are analysed for the occurrence of drilling-induced fractures between 3000 and 4000 m depth. Apart from local variations the orientation of the drilling-induced fractures is constant with depth and has a mean value of N154° ± 17°.

The number of drilling-induced tensile fractures occurring with depth varies significantly in all three boreholes. Figs. 3–5 present the depths, occurrence and orientation of the fractures with depth for the KTB pilot hole, the KTB main hole and the GPK1 hole, respectively. The data presented in Fig. 5 for the GPK1 hole consist of two data sets, the data above 1950 m depth are analyzed by Tenzer et al. [20] from borehole televiewer logs, the data below this depth by Nagel [21] from FMS logs. All three wells are characterized by sections with very frequent drilling-induced tensile fractures interrupted by sections with very few. There is no systematic decrease or increase of the number of fractures with depth. Below 5500 m depth in the KTB main hole data quality is often quite poor (indicated by horizontal bars on the right hand side of Fig. 4) and the fractures displayed in Fig. 4 may not represent the true number of drilling-induced tensile fractures. Comparison of the depth distribution of breakouts and tensile fractures in the KTB holes demonstrates that over large sections the borehole is failing both in compression and tension. In the Soultz-sous-Forêts GPK1, well tensile fractures are intermittently present over the entire section under investigation but are significantly more frequent between 2100 and 2400 m and between 3000 and 3200 m (Fig. 5). In contrast to the KTB holes the GPK1 hole is not failing in compression as no wellbore breakouts were detected in the hole [20].

2.1. Evidence for drilling related origin

Several observations strongly support that the tensile fractures are created during the drilling process and are not preexisting features crosscut by the well. As mentioned above, in sections of the KTB pilot well which were cored and where logging indicates vertical fractures, the cores do not show these fractures. In contrast, natural fractures seen at the borehole wall with logs are always seen in the core. In some cases, so-called centerline fractures were found in the cores [22]. They have the same orientation as drilling-induced fractures, are fresh and show no mineralization. These are interpreted as initiated by stress relaxation during the retrievement of the core from the respective depth of origin and are not seen in the FMS/FMI logs.

Drilling-induced tensile fractures were also recognized in Borehole Televiewer (BHTV) images in the KTB main well. The analysis of these images adds additional evidence to the initiation of the vertical fractures by the drilling process and their relation to the stress field around the wellbore. Like in the FMS/FMI-images, the vertical fractures are seen to be linear structures of 0.1–2 m length, parallel to the wellbore axis at diametrically opposed sides of the wellbore wall. This can be clearly seen with the BHTV as it records a full 360° image of the borehole wall. Most striking and most important for the further work with these structures is their orientation with respect to the breakouts [19]. The vertical tensile fractures occur at exactly 90° to the orientation of the breakouts (but generally not at exactly the same depth as the breakouts which means that the elastic solution for the stress around a cylindrical opening is still a valid description of the stress field). As breakouts are oriented in the direction of the least horizontal principal stress S_h this is direct evidence that the tensile fractures are oriented in the direction of the greatest horizontal principal stress S_H. A further argument for the initiation of these fractures during the drilling process is their relative abundance. As it is very unlikely to hit fractures which are parallel to the wellbore axis, the interpretation of the vertical fractures as preexisting natural fractures, would imply a vast population of preexisting vertical fractures, which is not considered to be likely as no such fractures are observed in approximately 4000 m of continuous core from the KTB pilot hole.

2.2. KTB boreholes

The orientation of the drilling-induced fractures detected in the KTB pilot and main hole are displayed in Figs. 3 and 4, respectively. The drilling-induced tensile fractures determined in the KTB pilot hole between 3000 and 4000 m depth exhibit a mean orientation of 154° ± 17°N. Hydraulic fracturing experiments carried out in the pilot hole to a depth of ~3000 m resulted in a S_H orientation of 149° ± 15°N [23]. In the KTB main hole the mean

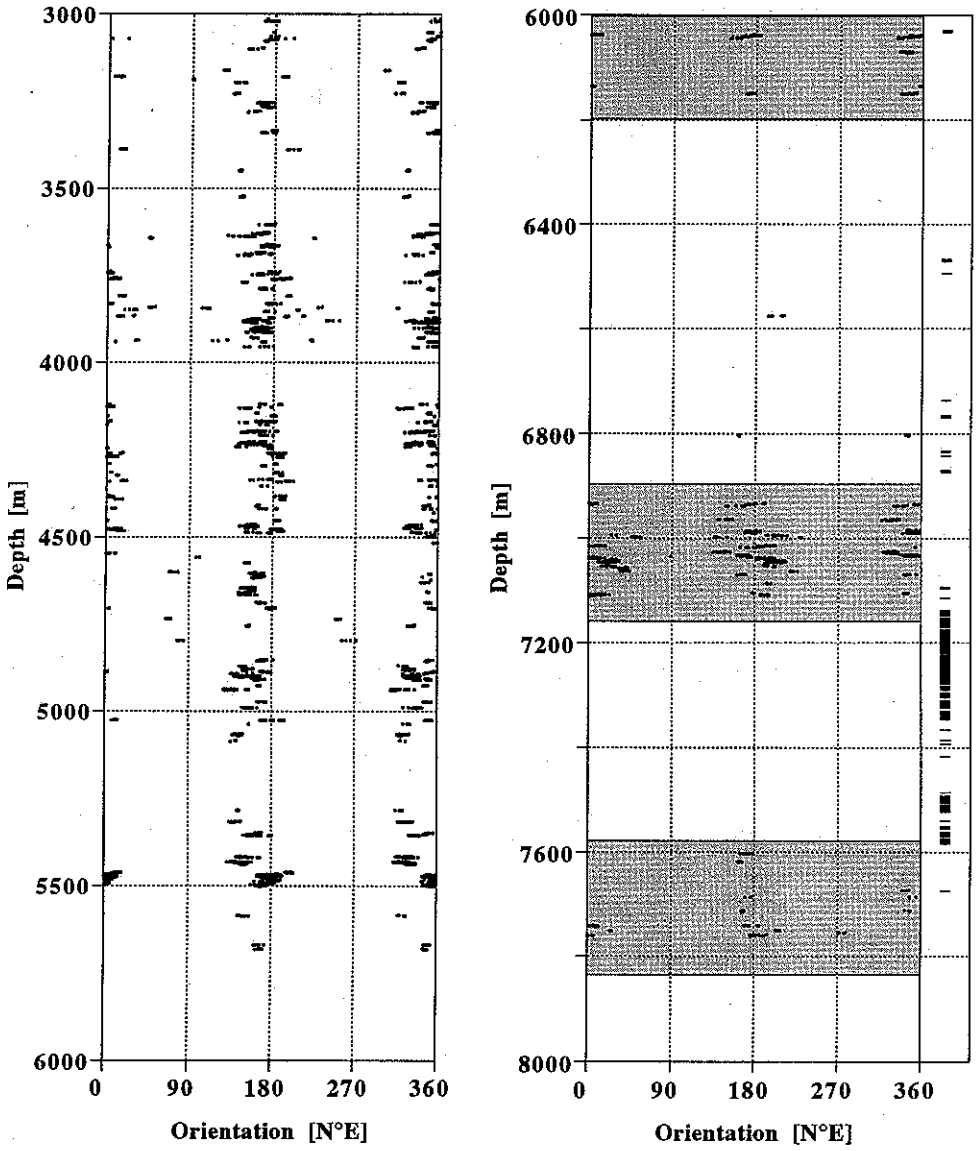

Fig. 4. In the KTB main hole FMI and HFMS measurements were analyzed for the occurrence of drilling-induced fractures between 3000 and 8700 m depth. Between 3000 and 6100 m the drilling-induced fractures exhibit a mean orientation of N166° ± 17°, whereas the fractures detected at 7000 and at 7700 m have a mean orientation of N182° ± 21° and of N176° ± 11°, respectively. At the right hand side of the figure horizontal bars indicate depth sections where the image quality is poor due to the fact that the arms of the tool are not attached to the borehole wall. Therefore it can not be determined if there are no fractures or if they are just not visible in the images.

orientation of the drilling-induced tensile fractures between 3000 and 6100 m is 166° ± 17°N. The tensile fractures around 7000 and 7800 m are oriented 182° ± 21°N and 177° ± 11°N, respectively (Fig. 4) [19, 24].

An independent determination of the stress orientation was possible in the KTB holes by the analysis of borehole breakouts from BHTV images and four-arm caliper logs [19, 24, 25]. For the pilot hole a S_H orientation of 161° ± 14°N is found and for the main hole S_H orientations between 149° ± 18°N and 171° ± 17°N are determined with a trend to higher values for greater depth.

All these investigations show that the drilling-induced tensile fractures are occurring at an angle of 90° to the orientation of the breakouts as theoretically expected for tensile fractures at the borehole wall. This demonstrates that the initiation of the fractures is related to the stress-field and that the fractures can be used as reliable indicator for the orientation of the maximum horizontal principal stress.

2.3. Soultz-sous-Forêts GPK1 borehole

As no breakouts are found in the BHTV records the only source for direct determination of the stress orien-

tation in the GPK1 borehole is the analysis of drilling-induced tensile fractures. A first determination of the orientation of drilling-induced tensile fractures was carried out by Tenzer et al. [20] with BHTV recordings in the depth range 1450 to 2000 m. They found a mean orientation of S_H of 169°E ± 11°N (Fig. 5). In the depth range 2000 to 3590 m drilling-induced tensile fractures were analyzed from FMI measurements by Nagel [21] who derived a mean orientation of 181° ± 22°N for S_H.

3. Fracture traces inclined to the borehole axis

As mentioned above tensile fractures which are inclined to the wellbore axes were found in all three boreholes. Theoretically, this inclination can be caused by the well axis not being parallel to a principal stress [26]. This could mean either that the borehole is vertical like the KTB main well and the vertical stress is not a principal stress, or the borehole is deviated from the vertical direction if S_v is a principal stress. The analytical relations describing the stress field in an elastic medium around a wellbore that is not parallel to a principal stress direction were first developed by Hiramatsu and Oka [27] and Fairhurst [28]. Using these relations, Brudy and Zoback [17] calculated theoretical fracture traces for arbitrary borehole orientations for the case of a strike slip stress regime like it prevails at KTB [29] and Soultz-sous-Forêts [30–32] sites. They showed how an induced tensile fracture develops at an angle to the wellbore axis but does not propagate all around the wellbore. An image of such an fracture would show two traces diametrically opposed at the wellbore wall and separated by intact unfractured rock like those shown in Fig. 2. It should be noted that any of the 'vertical' fractures in the three wells were not absolutely straight and vertical but showed variations of a few degrees around the wellbore wall. These variations are probably due to inhomogeneities of the rock, and thus, these fractures are not regarded as truly inclined to the wellbore axis as the overall fracture trend is vertical.

Fig. 6(a) and (b) present the depths of occurrence and orientations of the inclined tensile fractures (crosses) compared to those of the vertical drilling-induced fractures (open squares) for the KTB pilot hole and the GPK1 hole, respectively. Obviously, the deviated fractures occur at the same azimuth as the vertical fractures and very few of the deviated fractures are at azimuths different than the orientation of S_H. As already discussed above, the orientation of the vertical fractures is controlled by the orientation of the tectonic stresses, which demonstrates that the orientation of the inclined fractures is also controlled by the tectonic stress field. The inclinations of the fractures with respect to the wellbore axes are presented in Fig. 7(a) and (b) with positive angles indicating a counterclockwise rotation of the fracture with respect to the borehole axis. The deviated fractures in the GPK1 well (Fig. 7b) are inclined to the borehole axis clearly below ~25°, whereas the deviated fractures in the KTB pilot hole (Fig. 7a) are inclined at greater angles (<45°). In the KTB pilot hole the gneisses encountered at the respective depth exhibit foliation which dips at angles between 30° and 60°, significantly shallower than the inclined tensile fractures. Thus, the inclined fractures seem not to use the foliation planes for their initiation.

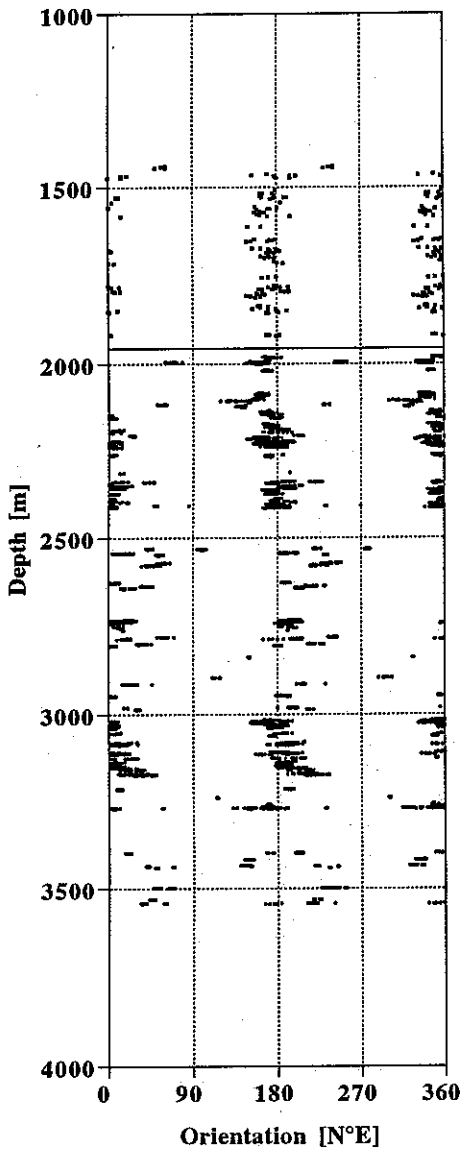

Fig. 5. The orientations of the drilling-induced fractures observed in the GPK1 borehole (above 1950 m [20] and below 1950 m [21]) seem to slightly turn to higher angles with depth. Overall, they indicate a N–S orientation of S_H.

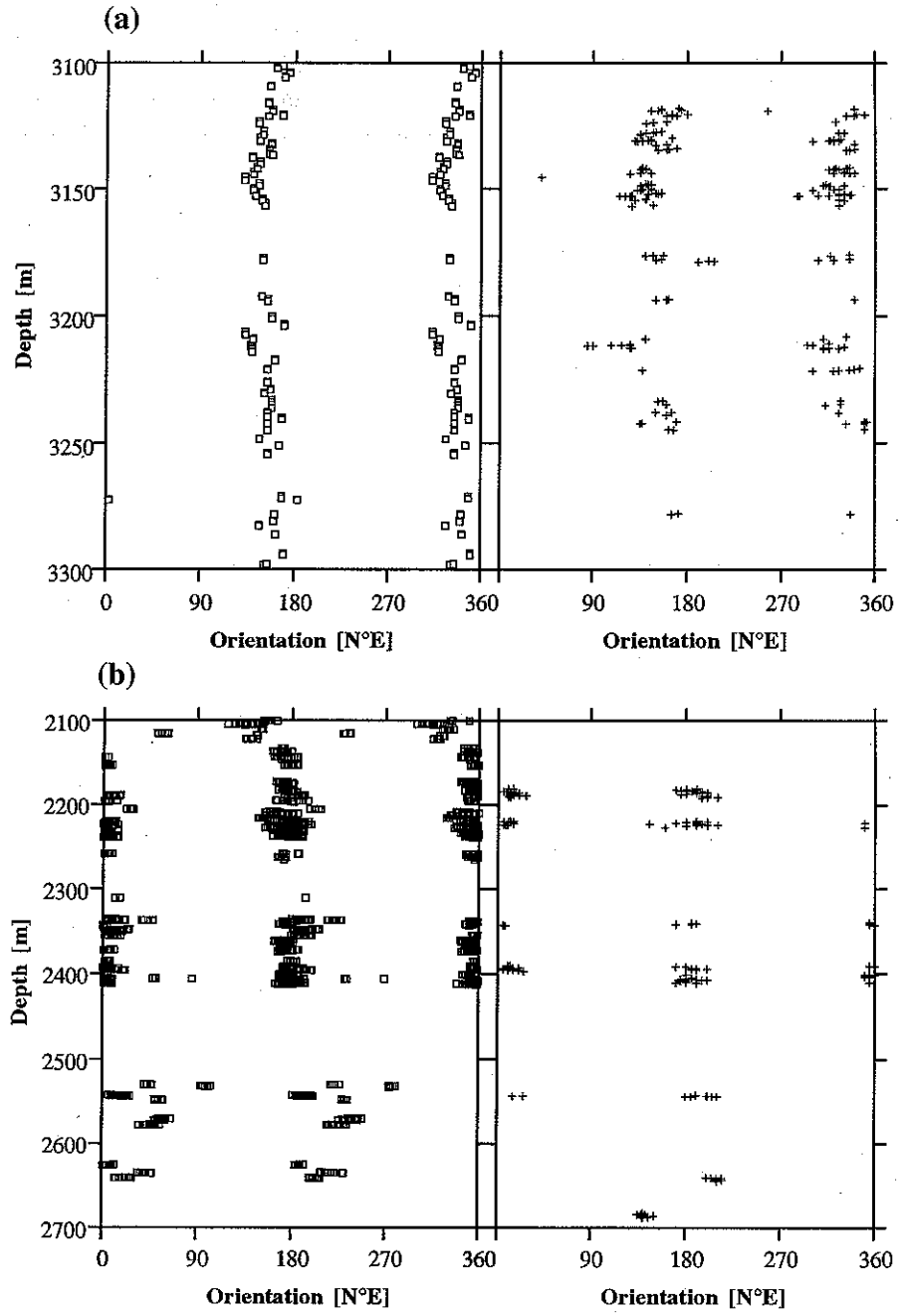

Fig. 6. Drilling-induced fractures inclined with respect to the borehole axis are found in (a) the KTB pilot hole between 3100 and 3300 m depth. Their orientation (crosses, right) is nearly identical to the orientation of the vertical fractures (open squares, left), which indicates that also the inclined fractures are controlled by the tectonic stress orientation. (b) Also in the GPK1 well at Soultz-sous-Forêts both populations (vertical fractures, left, and inclined fractures, right) show the same orientation in most depth sections.

In both, the GPK1 and KTB pilot hole, the inclined fractures are restricted in their occurrence to limited depth sections. In the GPK1 well the inclined fractures are clearly associated with natural faults crosscutting the borehole and are restricted to their close surrounding along the borehole. In some cases a gradual change of the fracture orientation with respect to the wellbore axis can be seen while approaching the fault. Shamir and Zoback [33] describe rotations of breakouts in the Cajon Pass scientific borehole in California and explain them by slip on faults which changes the stress field close to these faults. Similar rotations of breakouts have been described for the KTB pilot hole and the KTB main hole [19] and for several other wells in the United States [26] and in Russia [34]. All this evidence suggests that also deviated drilling-induced frac-

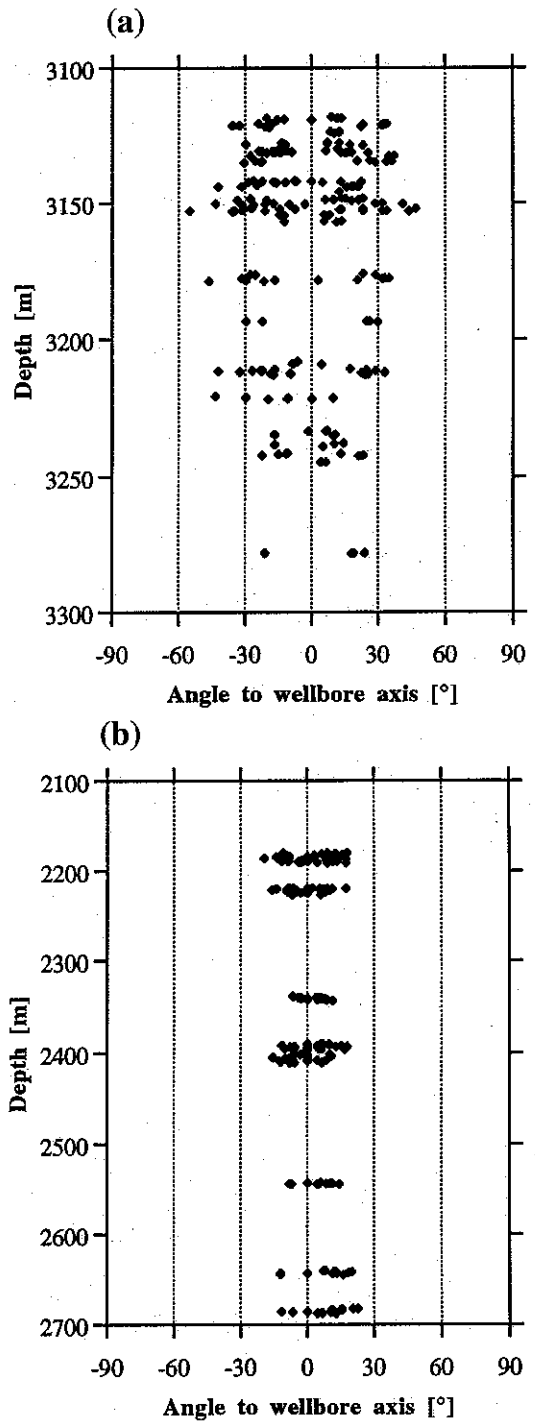

Fig. 7. (a) The angle of the inclined fractures with respect to the wellbore axis ranges in the KTB pilot hole between absolute values of 40° to 0°, which corresponds to dip angles of 50° to 90°. The foliation in the same depth section is dipping shallower at 30° to 60°. (b) The deviated fractures found in the GPK1 hole enclose angles of 30° to 0° with the direction of the wellbore axis, which indicate very steep dip angles of 60° to 90°.

tures are related to stress changes associated with slip on faults crosscutting the borehole. Theoretical work presented by Brudy and Zoback [17] and Peska and Zoback [35] allows the estimation of the angle β by which the principal stress axis deviates from a vertical from the angle ω_0 that the fracture makes with the vertical borehole axis. For ω_0 values between 10° and 30° (as determined for most of the deviated fractures in the KTB pilot hole and the GPK1 well) angles of β between 5° and 25° are found.

Of greater importance and interest is the fact that along most parts of both boreholes (as well as in the KTB main borehole to 7800 m depth) the drilling-induced tensile fractures are generally parallel to the borehole axis and thus indicate that in general, the vertical stress is a principal stress.

4. Initiation of vertical drilling-induced tensile fractures

To discuss the initiation and development of the drilling-induced tensile fractures we assume in the following that the vertical stress is a principal stress and that the borehole axis is vertical. Cases where these assumptions do not hold are discussed separately below. We further assume that the stress field around the wellbore can be described by the analytical solution given by [36] for the stress field around a circular opening in an elastic, isotropic infinite plate which is loaded by the far field principal stresses S_H and S_h. Anisotropy of the elastic properties of the rock is of secondary importance and therefore neglected.

4.1. Model for initiation

As explained in Section 3, we think there is convincing evidence that the vertical fractures are induced during the drilling process as pure mode I tensile fractures. In the following we discuss the fracture initiation for the case of the KTB main hole, which is drilled straight and vertical over the depth section of our investigation. This fact is significant as we assume in this part of the analysis that the vertical stress is a principal stress.

Drilling a hole in a pre-stressed ideally elastic medium leads to a stress concentration around the wellbore as first described by Kirsch [36] giving the stress as a function of angular position and radial distance from the center of the wellbore for a circular hole in an elastic plate. Maximum and minimum tangential stresses $\sigma_{\theta\theta}$ are reached directly at the wellbore wall, for $\theta = \pi/2$, $3\pi/2$ and $\theta = 0$, π, respectively, where θ represents the angle with respect to the orientation of the greatest horizontal principal stress S_H and P_0 is the pore pressure in the formation and ΔP the difference between the mud pressure P_b and the pore pressure P_0.

$$\sigma_{\theta\theta} = S_H + S_h - 2(S_H - S_h)\cos 2\theta - 2P_0 - \Delta P$$

The creation of breakouts in the direction of the minimum principal horizontal stress S_h due to the compressive tangential stresses at the wellbore wall overcoming the compressive strength of the rock are well described and commonly used to determine the stress orientation [1,2]. 90° from this direction, in the direction of the maximum horizontal principal stress S_H, the tangential stress becomes minimum. If Eq. (1) for the tangential stress which also forms the basis for hydraulic fracturing stress measurements [7,8] is valid, mode I fractures at the borehole wall can be initiated.

$$\sigma_{\theta\theta} = 3S_h - S_H - 2P_0 - \Delta P \leq T \quad (1)$$

In addition to the tectonic stress state, physical conditions during drilling, as the mud pressure in the wellbore P_b and the thermally induced stress σ_T associated with cooling the hole by circulation of relatively cold drilling mud, can significantly influence the formation of fractures. As the initiation of drilling-induced fractures is similar to initiation of a hydraulic fracture, we can use a 'breakdown-equation' as given by Hubbert and Willis [7] and Haimson and Fairhurst [8] including the thermally induced stress σ_T to take into account all stresses involved in the initiation of drilling-induced tensile fractures (see Ref. [37]). Nur and Byerlee [38] state that in rocks with low porosity the pore pressure plays a negligible role and Schmitt and Zoback [39] demonstrate experimentally that pore pressure is significantly diminished under rapid loading conditions in low permeability rocks. As we are dealing in all three investigated boreholes with rocks of low porosity and low permeability the pore pressure may be neglected and Eq. (1) changes into

$$\sigma_{\theta\theta} = 3S_h - S_H + \sigma_T - P_b \leq T$$

or

$$3S_h - S_H + \sigma_T - P_b - T \leq 0 \quad (2)$$

Eq. (2) is the condition which has to be satisfied in order to initiate drilling-induced fractures.

The downhole mud pressure P_b acting on the borehole wall at a given moment during drilling is the sum of the hydrostatic pressure P_{hydr} of the drilling mud and the dynamic pressure surges associated with the mud pumps. In the following, we estimate both the downhole mud pressure and the thermally induced stress which acts on the borehole wall and by combining these results with the magnitudes of S_H and S_h determined by hydraulic fracturing experiments in the KTB pilot hole, we will be able to check if the available stresses are able to cause the initiation of tensile fractures as predicted by Eq. (2). It should be noted that we present a completely independent analysis of drilling-induced tensile wall-fractures based on linear elastic fracture mechanics below.

4.2. Downhole mud pressure P_b

The drilling mud used in the KTB-HB is a colloid of the synthetic phyllosilicate Hectorit (Dehydril-HT), with its viscosity depending on the rate of flow [40]. Highest viscosity is reached at low flow velocities and gel structures (thixotropy) occur if there is no flow.

The pumping pressure during the drilling operation is recorded at the surface, P_{surf}. To determine the pressure at the bottom of the well, dynamic pressure losses in the drillpipe have to be taken into account. In the case of Dehydril, the highest pressures are reached when the pumps are started. This pressure peak is assumed to be transmitted throughout the mud column with only minor losses because initially there is no movement of the mud (the mud is a thixotropic gel) and dynamic pressure losses are negligible. We used 95% of the maximum wellhead pressure (when the pumps were started) for our further calculations as an estimate of the maximum dynamic pressure. Thus the downhole pressure is the sum of the hydrostatic pressure P_{hydr} and 95% of the well-head pressure P_{surf}. For the type of analysis we are carrying out the maximum pressure a given section of rock has experienced after drilling and before the fracture was detected by logging needs to be determined. For this purpose it has to be taken into account that pressure peaks recorded when the borehole had reached a certain depth raise the pressure also in the entire mud column

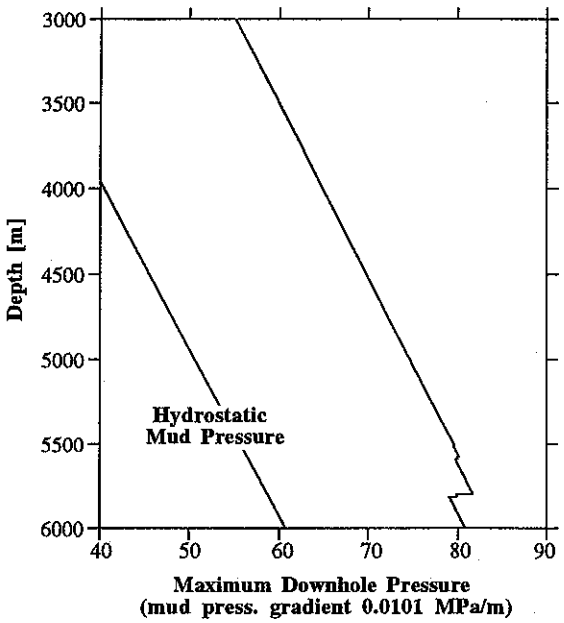

Fig. 8. The maximum downhole pressure a borehole section ever stands before the FMS/FMI measurements are run is calculated as the sum of the hydrostatic mud pressure and the highest surface pumping pressure before this time. The average maximum downhole pressure is about 25 MPa greater than the hydrostatic mud pressure at the respective depth.

above this depth and can overcome the pressure recorded for these shallower depth sections at earlier times. The values for the maximum downhole pressure range between 42 and 52 MPa and are shown in Fig. 8.

For common oil- or water-based muds, the dynamic pressure losses in the drilling equipment (drill string, bit-nozzles) have to be calculated. This is done below for the study of the drilling-induced fractures in the GPK1 well, where a salt water mud with a density of 1.07 g/cm^3 is used.

Running in the drillpipe causes a pressure increase below the bit due to a piston effect (swab pressure). For the boreholes discussed in this study the pressure increase connected to this effect is small compared to the pumping pressure and compared to the effect of cooling and is thus neglected. For different drilling equipment and borehole conditions this effect may cause a significant pressure increase and thus needs to be considered when analysing drilling-induced fractures.

4.3. Thermal stress

The borehole wall and the surrounding rock mass in the lower part of the KTB main borehole are strongly cooled by the drilling mud, which is pumped into the borehole at nearly surface temperature. On the way down to the drillbit the temperature of the mud increases but does not reach the undisturbed temperature of the rock and is therefore capable of extracting appreciable heat from the rock. The radially-varying temperature field around the borehole caused by this effect depends on the thermal diffusivity of the rock, the radius of the borehole and the time since cooling started. Integrable expressions for the temperature field around a cylindrical borehole in a infinite medium are given by Ritchie and Sakakura [41] for times of approximately one day through infinity. The stresses resulting from a radially-varying temperature field are derived by Nowacki [42] and specified for the case of a cylindrical borehole by Stephens and Voight [43]. For the consideration of fracture initiation only the stress directly at the borehole wall is of importance and can be calculated by the simple expression

$$\sigma_T = -\frac{\alpha E \Delta T}{1-\nu} \tag{3}$$

The calculation of the thermal stress according to Eq. (3) involves the determination of the linear coefficient of thermal expansion α, the Young's module E, the Poisson ratio ν and the temperature difference ΔT between the undisturbed temperature of the rock and the temperature after circulation of the drilling-mud.

The coefficient of thermal expansion of a rock is best represented by the average of the coefficients of thermal expansion of the minerals constituting the rock [44]. The abundances of quartz, mica, amphibolite, garnet, chloride, biotite, muscovite and plagioclase are analyzed routinely in the KTB holes and offer the possibility to calculate the coefficient of thermal expansion from the mineral composition. Except for quartz (1.0×10^{-5}/K), all these minerals have a very similar coefficient of thermal expansion (about 0.6×10^{-5}/K), which allows calculation of the linear coefficient of thermal expansion for the rock by the following formula:

$$\alpha = \mathrm{cont_q}\alpha_q + (1-\mathrm{cont_q})\alpha_{\mathrm{others}} \tag{4}$$

where $\mathrm{cont_q}$ is the quartz content, α_q is the coefficient of thermal expansion of quartz and α_{others} the coefficient for the other minerals. The resulting coefficients of thermal expansion (Fig. 9) may differ to some minor extent from the actual in-situ thermal expansion of the rock. The reason for this is twofold, first the volumetric expansion is not only caused by the expansion of the minerals but also by the creation of new porosity due to different expansion coefficients of the various mineral grains and second the values for the expansion coefficients are determined for constant pressure and therefore do not reflect the dependence of thermal expansion on the pressure.

The elastic parameters Young's modulus E and Poisson ratio ν are derived from P- and S-wave sonic velocities measured in the direction parallel to the borehole axis as an average value for all azimuths

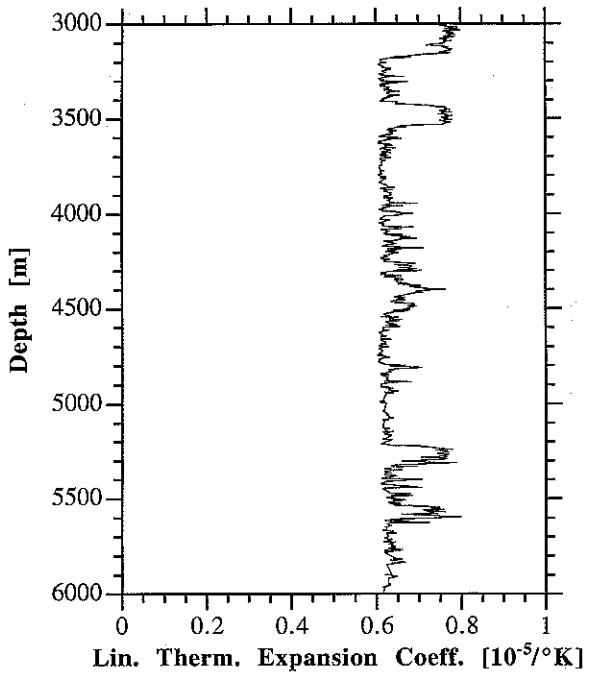

Fig. 9. The linear coefficient of thermal expansion α is calculated for the appropriate mineral composition according to Eq. (4). The sharp lower bound at 0.6×10^{-5}/K corresponds to the coefficient of thermal expansion for common minerals except quartz.

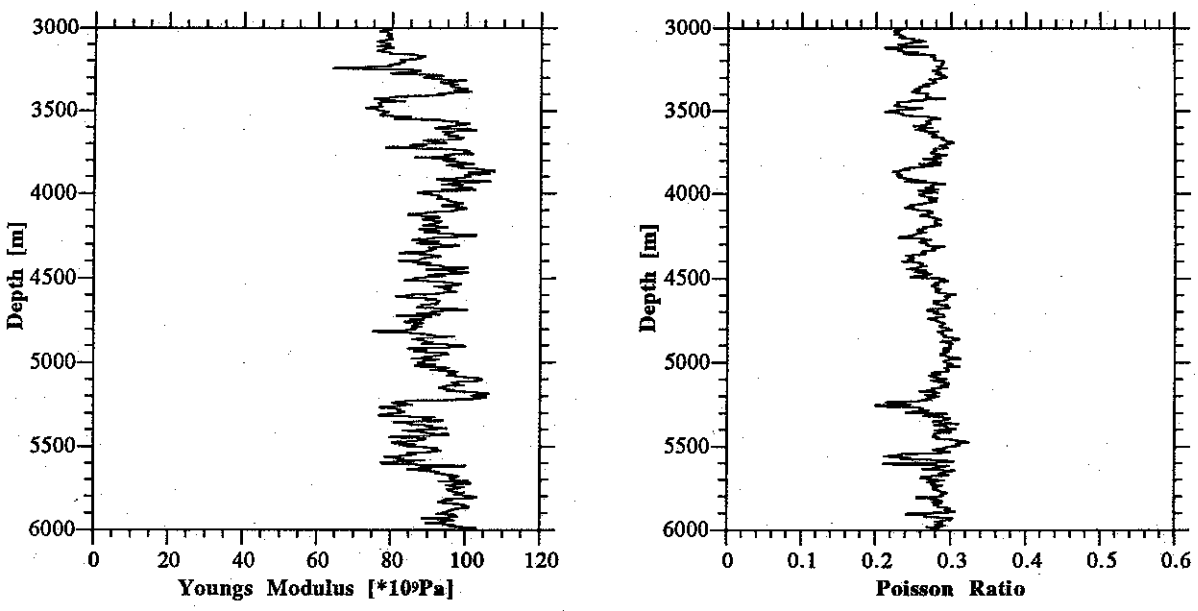

Fig. 10. Young's modulus E and Poisson ratio ν are computed from P- and S-wave sonic velocities.

around the wellbore. Resulting Young's modulus and Poisson ratio are plotted in Fig. 10.

The undisturbed temperature of the rock is derived from temperature measurements after borehole equilibration which lead to a temperature gradient of 28 K/km [45]. To find the amount of drilling-induced cooling of the rock temperature, thermal logs carried out during measurement phases were compared to the equilibrium temperature profile. As the temperature logs were carried out several hours after circulation was stopped, the temperatures found in these logs are slightly higher than the temperatures during drilling. In the KTB main well where both temperature logs and temperature measurements while drilling are available, it is shown that the steep temperature gradient in radial direction around the wellbore, produced by the drilling process, allows the drilling mud and the borehole wall to significantly heat up in short time periods after the end of circulation. The resulting thermal stress in the KTB main hole ranges between −15 and −60 MPa and is presented in Fig. 11.

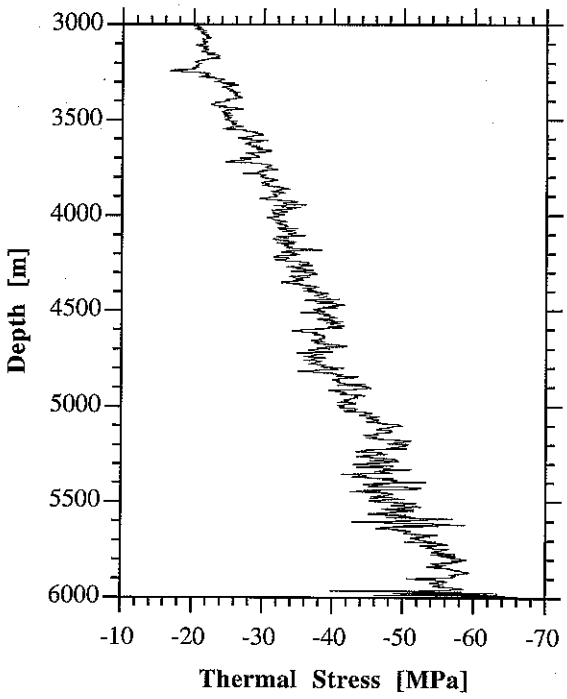

Fig. 11. The resulting thermal stress α_T calculated after Eq. (3) ranges between −15 and −60 MPa.

As no measurements while drilling are available for the pilot hole we used the difference between the temperature logs run between the drilling phases and the undisturbed formation temperature to estimate the maximum amount of cooling the rock experienced. This is a conservative estimation of the cooling and thus of the thermally induced stress because the true cooling has probably been a few degrees more.

4.4. Tensile strength

In classical hydraulic fracturing theory it is assumed that in order to initiate a fracture the tensile strength of the rock has to be overcome (tensile strengths of rocks from KTB are around 10 MPa) [46,47]. This is due to the fact that hydraulic fracturing experiments are usually made in sections of the borehole which do not contain pre-existing natural fractures. In contrast to this, drilling-induced fractures are initiated most easily if small flaws in the borehole wall can be used as starting points for the development of fractures

Table 1
Compilation of the results of hydraulic fracturing investigations carried out 1991 and 1992 in the wells EPS1 and GPK1 in Soulz-sous-Forêts, France

Well/date	Depth (m)	S_h (MPa)	S_H (MPa)
EPS1/1991	2195	26.6	50.2
EPS1/1991	2205	27.0	54.8
GPK1/1992	3315	45.2	91.3
GPK1/1992	3506	44.2	87.4

because just there no tensile strength has to be overcome. Thus, we assume that the tensile strength of the rock can be neglected for the analysis of drilling-induced fractures.

5. Confirmation of proposed model for fracture initiation and estimation of S_h magnitude from analysis of drilling-induced tensile fractures

Magnitudes of the horizontal principal stresses S_h and S_H determined by hydraulic fracturing in the GPK1 well and in the KTB pilot hole allow to demonstrate that the initiation of drilling-induced fractures can be described by the model proposed above. This model also offers the opportunity to estimate the magnitude of S_H if S_h is known from any other stress measurement method. Using Eq. (2) it can be argued that fractures initiate first if the tangential stress at the borehole wall σ_{00} is equal to zero. Solving Eq. (2) for S_H with the assumption of negligible tensile strength T leads then to

$$S_H = 3S_h + \sigma_T - P_b \quad (5)$$

which allows calculation of the minimum magnitude of S_H necessary to initiate fractures for a given magnitude of S_h, thermal stress σ_T and borehole pressure P_b. The congruence between results from hydraulic fracturing measurements at 3 km depth in the KTB pilot hole and the estimation of the magnitude of S_H with the method proposed above confirm that this method is capable of estimating reasonable stress magnitudes. Finally, the magnitude of S_H is estimated applying this new method in the KTB main hole to 6 km depth.

5.1. Soultz-sous-Forêts boreholes: confirmation of fracture initiation model

In 1991 and 1992 hydraulic fracturing measurements were conducted in the well GPK1 and in a nearby well EPS1. Table 1 summarizes the results from these measurements. The magnitudes of S_h and S_H are shown in Fig. 12 by squares and triangles, respectively. The vertical stress S_v is calculated as the gravitational load of the rock with a density of 2.45 g/cm^3 for the sedimentary cover and 2.55 g/cm^3 for the granite. The stress magnitudes indicate a stress regime in transition from normal faulting to strike-slip ($S_H \sim S_v$) which is consistent with the tectonic situation in the Rhine Graben and with other stress measurements in this region [30–32].

A determination of the thermally induced stresses and the pumping pressures acting at depth results in values of up to 12 MPa for the thermal stress but negligible values for the downhole pumping pressure. The dynamic pressure losses in the drill pipe and in the bit-nozzles are so high that only an additional pumping pressure of less than ~2 MPa is acting on the borehole wall. The evaluation of the hydraulic fracturing experiments indicates that the tensile strength T of the rock is very small [48] and thus can be neglected investigating the initiation of tensile fractures. Instead of using Eq. (2) to calculate the tangential stress $\sigma_{\theta\theta}$ in the borehole wall with the above derived values of σ_T, P_b, T and S_H and S_h derived from hydraulic fracturing, Eq. (5) and interpolated values of S_h are used to derive S_H curves. The lower bound estimation (curve 1 in Fig. 12) uses the assumption that the fractures developed with the help of the thermal stress ($S_H = 3S_H + \sigma_T - P_b$), whereas curve 2 assumes that the hydrostatic mud pressure and the tectonic stresses were sufficient to cause the fractures ($S_H = 3S_H - P_{hydr}$).

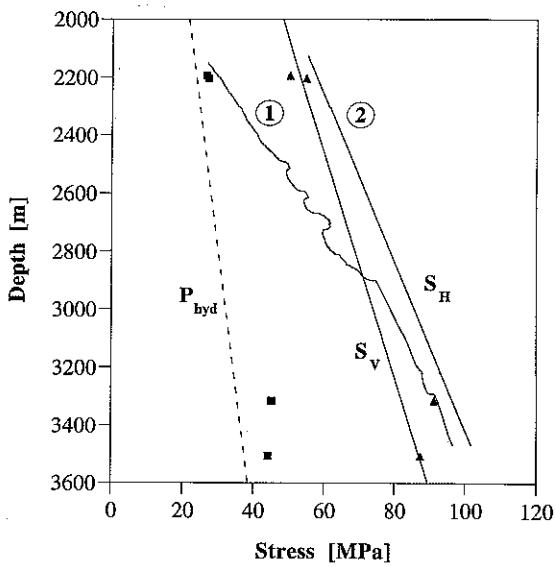

Fig. 12. S_h and S_H magnitudes derived from hydraulic fracturing experiments in the boreholes at Soultz-sous-Forêts are displayed as squares and triangles, respectively. Curve 1 represents the estimation of the magnitude of S_H assuming that the initiation of the fractures is supported by thermally induced tension at the borehole wall, whereas curve 2 represent the estimation for the assumption that no additional stresses besides the tectonically induced stresses caused the formation of the fractures. The estimated stress magnitudes are in very close agreement with the results found in hydraulic fracturing experiments in the GPK1 and in the close EPS1 borehole.

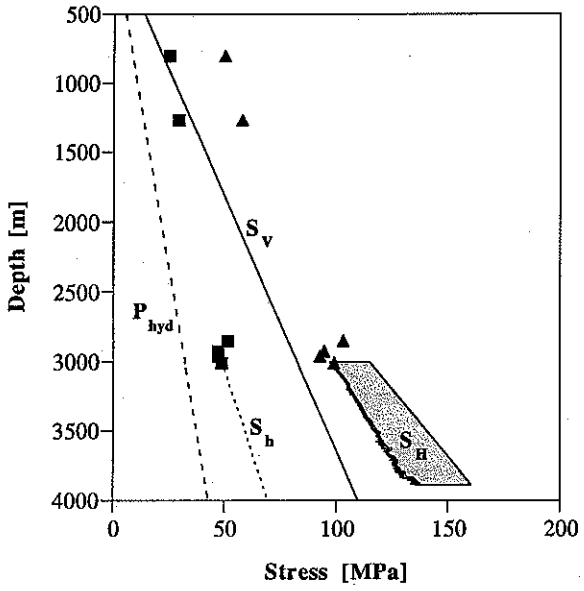

Fig. 13. S_h and S_H values determined by hydraulic fracturing experiments in the KTB pilot hole are marked by squares and triangles, respectively. Estimation of the magnitude of S_H using the analysis of drilling-induced fractures in the KTB pilot hole leads to the grey-shaded range of S_H-magnitudes. The estimation is at very good agreement with the results from the hydraulic fracturing experiments at about 3 km depth.

Results from hydraulic fracturing are available at the upper and lower end of the depth section we investigated for drilling-induced tensile fractures. Three out of the four S_H magnitudes determined by hydraulic fracturing (Fig. 12) lie inside or very close to the estimated range of S_H magnitudes. This means that according to our model describing the fracture initiation the observed stress states allow the development of fractures which are actually observed (Fig. 5). It also confirms that (1) the model we use is able to explain the initiation of the fractures and (2) the assumption of negligible tensile strength is valid.

5.2. KTB boreholes: estimation of S_H magnitudes

In the KTB pilot hole hydraulic fracturing experiments were carried out between 800 and 3011 m depth [23] and in the KTB main hole at 6000 m depth [29,49]. The standard hydraulic fracturing tests in the pilot hole yielded values of the magnitude of both the minimum and maximum horizontal principal stress, whereas the modified test in the main hole only allowed limiting a range of possible magnitudes of S_h.

[2] Combined analysis of compressive failure of the borehole wall (breakouts) and drilling-induced fractures indicates that the actual magnitude of S_h is very close to the lower limit found in the modified hydraulic fracturing test at 6 km depth. Therefore, we think it is reasonable to interpolate the S_h magnitudes in the way described.

The resulting magnitudes of S_h and S_H are presented in Figs. 13, 14 and 16 by squares and triangles, respectively.

In the depth range from 3000 to 4000 m in the KTB pilot hole we confirm by comparison of the estimated magnitudes to the results obtained from hydraulic fracturing that the newly proposed method for estimation of the S_H magnitude is working. For this purpose the magnitude of S_h is calculated as the linear interpolation of the deepest hydraulic fracturing measurements in the pilot hole and the lower bound value for S_h at 6000 m in the main hole[2]. The estimated range of S_H magnitudes is given in Fig. 13 by the grey-shaded area marked S_H. The lower boundary results from the assumption that both thermal stress due to cooling and pumping pressure act together on the borehole wall to create the fractures. The upper bound assumes that none of these additional stresses is present to initiate the fractures. Thus, this line is given by

$$S_H = 3S_h - P_{hydr}$$

At 3011 m the lower bound of the estimated range for the magnitude of S_H is identical with the S_H magni-

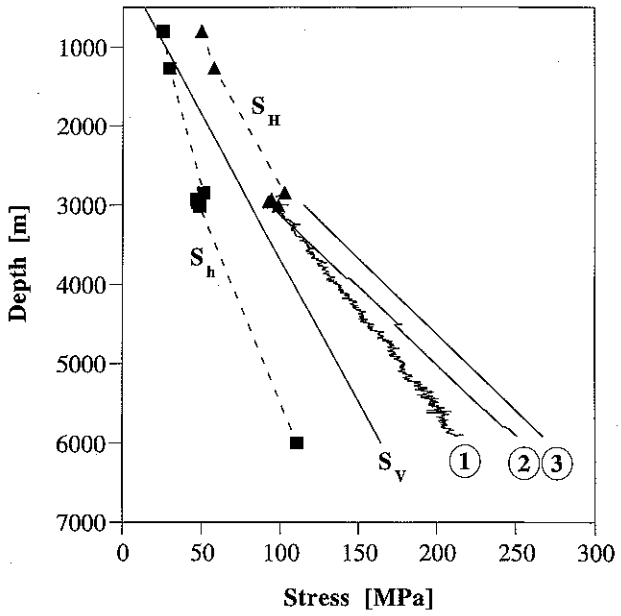

Fig. 14. S_h and S_H values determined by hydraulic fracturing experiments in the KTB pilot hole are marked by squares and triangles, respectively. Curves 1–3 are lower bounds for the magnitude of S_H estimated from the analysis of drilling-induced fractures in the KTB main hole. For curve 1 it is assumed that the fractures are initiated when the thermal stress due to cooling of the rock plus the hydrostatic mud pressure were acting, for curve 2 the maximum surface pumping pressure plus the hydrostatic mud pressure were assumed to be acting, while for curve 3 only the tectonic stresses are assumed to be acting. Also in this analysis there is good agreement between the estimation and the results from the hydraulic fracturing experiments at 3 km depth.

tudes determined in hydraulic fracturing tests at this depth. This indicates that (1) this new method is capable of providing reliable estimates of the magnitude of S_H, (2) the fractures in the pilot hole initiate only if both pumping pressure and thermal stress are acting on the borehole wall and (3) the rock has no tensile strength considering the initiation of drilling-induced tensile fractures. For comparison in Fig. 13 the hydrostatic pressure P_{hyd} and the vertical stress S_v are presented. In the depth range of the pilot hole the stress regime is a strike-slip faulting stress regime.

The estimation of the magnitude of S_H to 6000 m depth by analysis of drilling-induced tensile fractures is possible in the KTB main hole. The lower bound of the magnitude of S_h is known from hydraulic fracturing [29,49]. Fig. 14 summarizes the results of this investigation. The curves marked by the numbers 1 to 3 represent magnitudes of S_H necessary to initiate drilling-induced fractures for the following assumptions: (1) the maximum amount of cooling induced thermal stress σ_T and the hydrostatic pressure of the mud P_{hydr} are acting on the borehole wall, while no pumping pressure is available. (2) The maximum available pumping pressure P_{surf} plus the hydrostatic pressure of the mud P_{hydr} is acting on the borehole wall, while no thermal stress is present. (3) Only the hydrostatic mud pressure P_{hydr} is acting on the borehole wall. Estimating of the magnitude of S_H in the KTB pilot hole we assumed that both pumping pressure and thermally induced stress act at the same time and gained reasonable estimates of the stress magnitude. In the case of the KTB main hole it is more realistic to separate both influences. The pumping pressure is highest when the pumps start and the pressure pulse is transmitted down the well with only minor losses (caused by the rheology of the thixotropic mud), whereas the thermally induced stress becomes most important with drilling time when the cooling of the rock becomes greater. In the KTB pilot hole the same type of mud as in the KTB main hole is used and therefore the same arguments could be applied, but it turns out that splitting the influences would not significantly change the result as the thermally induced stress there is only about 5 MPa. This means by separating the influences the lower boundary for the S_H magnitude would raise by only about 5 MPa. Therefore, not separating the two influences can be seen as using the lowest estimation.

In conclusion the investigation in the KTB main hole shows the continuation of a strike-slip stress regime, already found in the KTB pilot hole, to a depth of 6000 m. This is confirmed by the seismicity in the area and in the nearby Eger Graben [50] which also indicates a strike slip stress regime at the KTB site. The estimated range of magnitudes becomes wider but still allows conclusion on the tectonic style and the approximate magnitude of the shear stress present at depth.

6. Stress estimation using analytically calculated stress intensity factors

The analysis presented above is based on the description of tensile failure at borehole walls following Hubbert and Willis [7]. The initiation and growth of tensile fractures also can be described by the analysis of the stress intensity factor K_I which describes the stress concentration at the fracture tip which is responsible for either growth or stabilization of the fracture. If the stress intensity factor for certain loading conditions overcomes a critical value which is specific for the material and that is called either the critical stress intensity factor or fracture toughness K_{Ic}, the fracture grows. Appendix A shortly summarizes the derivation of the stress intensity factor for a fracture initiating at the borehole wall under the loads of S_H, S_h, mudpressure in the borehole and mudpressure inside the fracture [51,52]. Besides these loads also the stress induced by cooling of the rock during circulation is important for initiation and growth of fractures at the borehole wall, as was shown earlier in this paper. Therefore in Appendix A the stress intensity factor K_I for the thermally induced stress is derived and discussed. This new description of the drilling-induced tensile fracture allows two things, the estimation of a maximum length the fracture extends away from the borehole wall and an independent method to estimate the magnitude of S_H.

As above the minimum horizontal stress S_h is assumed to be known from hydraulic fracturing measurements and the value for the critical stress intensity factor K_{Ic} for crystalline rocks commonly ranges between 0.5 and 3 MPa $m^{1/2}$ [53,54]. As no direct measurement of this parameter for the rocks at KTB is available we chose a value of 1 MPa $m^{1/2}$ for K_{Ic} as representative.

Using Eq. (6) which is derived from Eq. (A.5) (Appendix A) the magnitude of the greatest horizontal principal stress can be estimated.

$$S_H = \frac{-S_h\sqrt{R}g(b) + p\sqrt{R}h_0(b) + p_a\sqrt{R}h_a(b) + D\sqrt{R}j(b) - K_{ic}}{\sqrt{R}j(b)} \tag{6}$$

g, h_b, h_a, j and f are the stress intensity functions for the loads S_h, p (pressure in the borehole), p_a (pressure in the fracture), D (thermal stress at the borehole wall) and S_H, respectively. Values used in this estimation for bitsize, time of cooling, critical stress intensity factor K_{Ic} and thermal diffusivity k are listed in Table 2.

Table 2
Input values used for the estimation of the magnitude of the greatest horizontal principal stress in 6 km depth

Bitsize ($=2R$)	$14\frac{3}{4}$ inch = 37.47 cm
Time of cooling	20 h
K_{Ic}	1 MPa $m^{1/2}$
κ	10^{-6} m^2/s

The stress estimation is carried out at four different depths 3, 4, 5 and 6 km. The values used for the least horizontal principal stress S_h, the mud pressure and the cooling are listed in Table 3.

Using Eq. (6) the results are dependent on the initial fracture length L we assume. Plotting S_H for relative initial fracture length up to 0.1 (corresponds to a relative radius of 1.1) (Fig. 15) the resulting curve always has a minimum in this interval and is monotonically increasing for greater relative radii. This means that there is a minimum value of S_H below which no fractures can be extended. At 3 km depth this minimum value is at 110 MPa and corresponds to an initial fracture length of 0.9 cm. For greater S_H shorter fractures can be used as initial fractures. Thus, the occurrence of drilling-induced fractures at a depth allows us to determine a lower bound for the magnitude of S_H from the analysis presented above. A comparison of the minimum values of the magnitude of S_H to the range of S_H magnitudes estimated previously (Fig. 16) demonstrates excellent agreement between the two methods. The estimation is carried out under the assumption that the mud pressure in the borehole is hydrostatic. Due to drilling activities the borehole wall probably experienced small pressure increases in the order of a few MPa's. Therefore the influence of such sudden pressure peaks on the estimation of the magnitude of S_H is checked. An increase of 10 MPa of the mud pressure at 6 km depth leads to a minimum value of S_H about 15 MPa lower than the minimum S_H value determined for hydrostatic pressure. This is a relatively small change which leads to an estimated S_H magnitude still in the range of the initial estimates.

To investigate the maximum radial extent of drilling-induced fractures the stress intensity factor K_I is

Table 3
Input values used for the estimation of the magnitude of the greatest horizontal principal stress in 6 km depth

Depth (m)	S_h (MPa)	Hydrostatic pressure (MPa)	Cooling (K)	Minimum S_H (MPa)
3000	48.5	30.3	42	110
4000	69.3	40.4	58	160
5000	90.0	50.5	75	209
6000	110.7	60.6	92	257

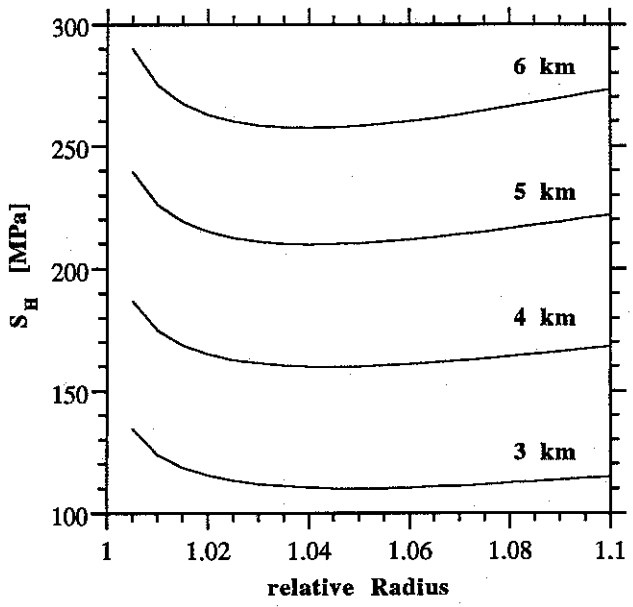

Fig. 15. S_H curves resulting from Eq. (6) for 3, 4, 5 and 6 km depth. All curves have a minimum in the plotted interval and are increasing monotonically for greater relative radii. For S_H values greater than the minimum value initial fractures can be extended.

plotted versus the relative radius for 3, 4, 5 and 6 km depth using the values given in Tables 2 and 3 (Fig. 17). From Fig. 16 minimum values for S_H are derived. If these values would be used to calculate K_I for the above mentioned conditions all the curves would tangent the line of K_{Ic} at one point. To really extend a initial fracture greater values of S_H are needed. To investigate the extension of drilling-induced fractures for

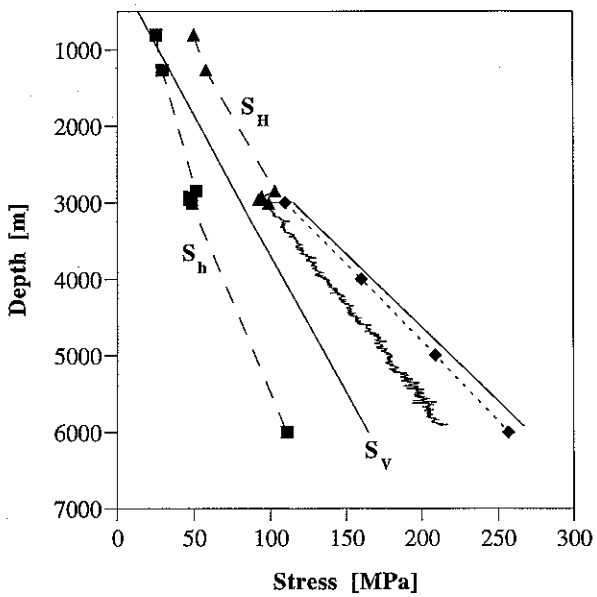

Fig. 16. The nomenclature for the stress values is the same as in Fig. 14. Additionally, the lower bounds resulting from Fig. 15 are plotted as filled quadrangles. These lower bounds fit inside the range of S_H values derived by the 'classical' analysis.

greater values of S_H we calculated K_I for S_H magnitudes that are 10 MPa greater than the respective minimum found from Fig. 16. The critical stress intensity factor K_{Ic} is marked by the dashed line at 1 MPa $m^{1/2}$. As the fracture stabilizes if the stress intensity factor drops below the critical value, the longest fracture can be created at 3 km with a relative length of 0.14 (corresponding in the KTB case to an absolute length of 2.6 cm). This result leads to the conclusion that even for higher S_H magnitudes still the drilling-induced fractures would be limited to the close proximity of the borehole wall.

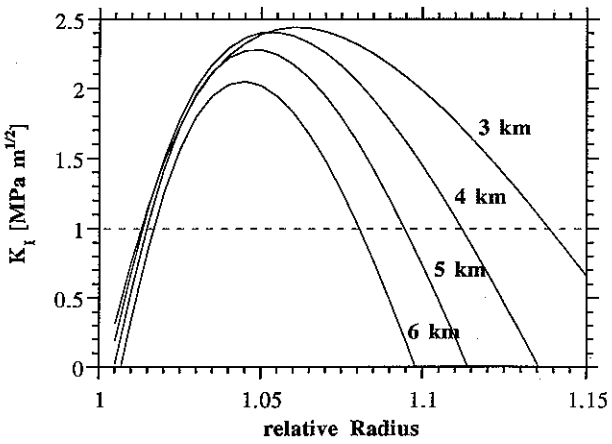

Fig. 17. Stress intensity values for 3, 4, 5 and 6 km are compared to the critical stress intensity factor (1 MPa $m^{1/2}$, dashed line) to estimate the maximum extent of drilling-induced fractures. The K_I curves are calculated for the values given in Tables 2 and 3 and for a magnitude of S_H that is 10 MPa greater than the minimum value of S_H found from Fig. 15. For these conditions the fractures are limited to the close proximity of the wellbore.

7. Conclusions

The theory presented for the initiation and development of the drilling-induced tensile wall-fractures is based on stress analysis for a linear elastic material using a strength of material approach for the initiation of the fractures. The initiation of the fractures can be explained taking into consideration the tectonic stress state, the downhole pressure acting on the borehole wall and the thermal stresses in the borehole wall induced by circulation of relatively cold drilling mud. This is shown by the fracture analysis in the GPK1 and the KTB pilot boreholes where the tectonic stresses were determined by hydraulic fracturing experiments in the investigated depth interval. We further show that the analysis of the fracture initiation yields a new estimate of the magnitude of the greatest horizontal principal stress S_H. The application of this stress measurement method to the KTB main hole allowed the determination of the S_H magnitude to 6 km depth.

Independently, fracture initiation is described by a more rigorous method calculating the stress intensity factor for the propagation of the drilling-induced fractures (Appendix A). This analysis allows estimation of the maximum extent the fractures reach away from the borehole wall. It is found that the drilling-induced fractures are constrained to the close proximity of the wellbore (much less than one borehole radius). Therefore, the possibility of mud losses through these fractures or significant influx due to connection to the natural fracture system is negligible. This method yields estimates of the magnitude of S_H within the bound given by the first estimate.

Acknowledgements

The authors like to thank J. Kück and M. Sowa for their continuous help in accessing the borehole measurements from the KTB boreholes and K. Huber for insightful discussions. The authors also wish to thank R. Nagel who analysed the FMI data from the GPK1 borehole for the occurrence of drilling-induced tensile fractures. Data from the KTB boreholes were kindly provided by NLfB-KTB and data from Soultz-sous-Forets by SOCOMINE. This work was financially supported by the Deutsche Forschungsgemeinschaft under grant FU55/31-5-6.

Appendix A. Fracture mechanics approach to the occurrence of drilling-induced fractures

A purely analytical fracture mechanics approach to the initiation of hydraulic fractures in a borehole was developed by Winter [51] and Rummel and Winter [52]. They treat hydraulic fractures as pure tensile fractures (mode I fractures). The stress intensity factor K_I for this fracture mode can be calculated as a superposition of the stress intensity factors resulting from various loading sources. Winter and Rummel present analytical expressions for the following loads:

- S_H, greatest horizontal principal stress.
- S_h, least horizontal principal stress.
- p_b, pressure of the drilling mud in the wellbore.
- p_a, pressure of the mud invading the fracture.

Also the initiation of drilling-induced fractures can be described by this theory, except an additional source of stress, the thermal stress due to circulation of relatively cold drilling mud, has to be taken into consideration. Thus, the existing theory of Winter and Rummel needs to be extended to include thermal stres-

ses around the borehole. In the following a short derivation of the stress intensity factor for the loads S_H, S_h, p_b and p_a [52] is presented and then the analytical expression for K_I describing the effect of thermal stresses around the borehole is derived and included into their formulae.

A.1. Derivation of K_I

The derivation of K_I is based on the general formulation of the stress intensity factor for a tensile fracture of half length L in an infinite plate given by Paris and Sih [55].

$$K_I = \frac{1}{\sqrt{\pi L}} \int_{-L}^{L} \sigma_y(x, 0) \left(\frac{L+x}{L-x} \right)^{1/2} dx \qquad \text{(A.1)}$$

This concept can be applied to a symmetrical fracture emanating from a pressurized borehole in an infinite elastic plate with the far-field stresses S_H and S_h (Fig. 18). The normal to the fracture plane of a fracture propagated in such a system will always be parallel to the direction of S_h. With the y-axis aligned with S_h and the x-axis with S_H, each of the above mentioned loads causes a normal stress σ_y on the fracture plane. For each load the loading function $\sigma_y(x, 0)$ and the respective integral (Eq. (A.1)) are calculated separately. K_I resulting from all loads is the sum of the integrals (Eq. (A.1)) calculated for the separate loads.

The stress intensity factor K_I for the influence of

(I) S_H, the greatest horizontal principal stress, is given by

$$K_I(S_H) = -S_H \sqrt{R} f(b)$$

$$f(b) = -2\sqrt{\frac{b^2 - 1}{\pi b^7}}$$

(II) S_h, least horizontal principal stress, is given by

$$K_I(S_H) = -S_h \sqrt{R} g(b)$$

$$g(b) = \sqrt{\pi b}\left(1 - \frac{2}{\pi} a \sin\left(\frac{1}{b}\right)\right) + 2(b^2 + 1)\sqrt{\frac{b^2 - 1}{\pi b^7}}$$

(III) p_b, the pressure of the drilling mud in the wellbore, is given by

$$K_I(p_b) = p_b \sqrt{R} h(b)$$

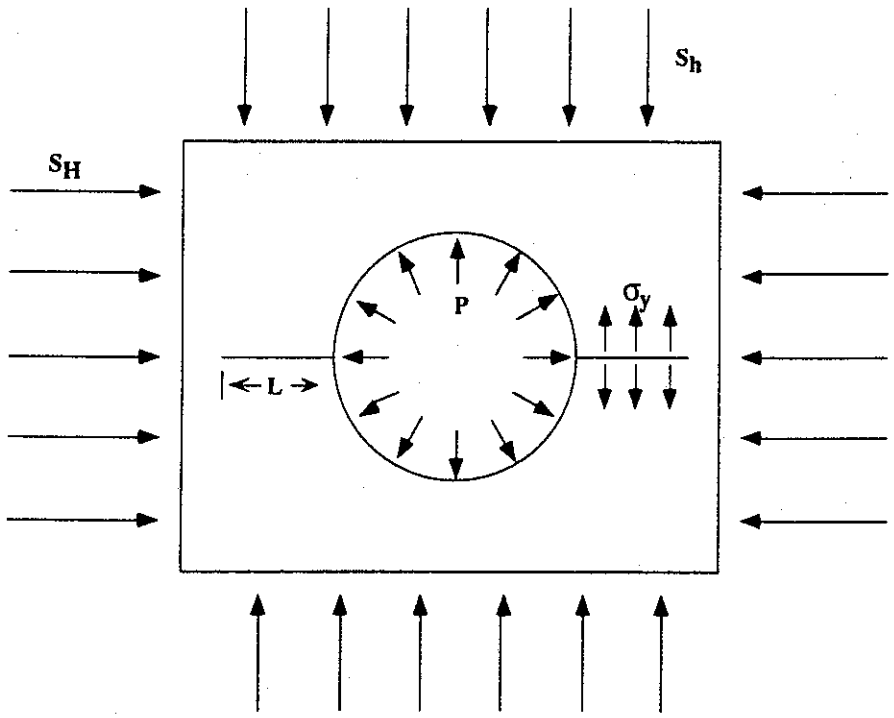

Fig. 18. A circular hole in an infinite plate with symmetrical fractures of length L. An internal pressure p_b is applied to the hole and the plate is loaded by the far field stresses S_H and S_h. For the calculation of the stress intensity factor for each load the stresses acting perpendicular to the fracture plane (σ_y) has to be determined.

$$h_b(b) = 1.3\frac{b-1}{1+b^{3/2}} + 7.8\frac{\sin((b-1)/2)}{2b^{5/2}-1.7}$$

(IV) p_a, the pressure of the mud invading the fracture, is given by

$$K_I(p_a) = p_a\sqrt{R}h_a(b)$$

A constant pressure p_a ($p_a = p_b$) equal to the pressure p_b in the borehole is assumed as pressure distribution inside the fracture for the results presented here. Stress intensity factors for other models of pressure distribution (linear, reciprocal and quadratic pressure drop) in the fracture are given by Rummel [56].

A.2. The effect of thermally induced stress

In boreholes at high temperatures, either deep boreholes or boreholes in regions with an elevated temperature gradient such as in geothermal fields, the rock can suffer a significant stress from cooling due to circulation of relatively cold drilling mud. The magnitude of the induced stress depends on the time of cooling, the temperature difference between formation and drilling mud and the thermal and elastic properties of the rock.

The cooling by the drilling mud introduces a radially varying temperature disturbance around the borehole. In order to determine the stresses caused by this disturbance an expression for the temperature field has to be found by solving the heat conduction equation. The problem can be described as an infinite conducting medium around a cylindrical inclusion of constant temperature [43]. A solution of the heat conduction equation useful to this problem is given by Ritchie and Sakakura [41]. The truncated version of this solution where ϑ is the actual temperature of the rock and ϑ_0 the undisturbed temperature of the rock

$$\frac{\vartheta}{\vartheta_0} = 1 + 2I_0^{-1}\ln\rho \quad \text{with } \rho = \frac{R}{x}$$

gives nearly identical results to the true solution, except for small values of ϑ/ϑ_0. ρ is the radius of the borehole R divided by the distance x from the center of the borehole ($\rho = R/x$). The function I_0^{-1} is derived from

$$I_m^n\left(\frac{4\tau}{\sigma_e^2}\right) = \frac{1}{2\pi i}\int_{-\infty}^{0+}\exp\left(\frac{4\tau}{\sigma_e^2}\right)z^{m-1}(\ln z)^n)\,dz$$

for $n = -1$ and $m = 0$ with

$$\tau = \frac{\kappa T}{R^2}, \quad \sigma_e = e^{\gamma}, \quad \gamma = 0.57722$$

τ is the Fourier number, which combines the time of cooling T, the thermal diffusivity κ and the borehole radius R. For I_0^{-1} we find the expression

$$I_0^{-1}\left(\frac{4\tau}{\sigma_e^2}\right) = \frac{1}{2\pi i}\int_{-\infty}^{0+}\frac{e^{(4\tau/\sigma_e^2)z}}{z\ln z}\,dz$$

After Spencer and Fano [57], I_0^{-1} can be calculated by the rapidly converging series

$$I_0^{-1}\left(\frac{4\tau}{\sigma_e^2}\right) = \frac{1}{\pi}a\tan\left(\frac{\pi}{B}\right) + \frac{\Gamma^{(1)}(1)}{(\pi^2+B^2)} + \frac{B\Gamma^{(2)}(1)}{(\pi^2+B^2)^2}$$

with

$$B = \ln\left(\frac{4\tau}{\sigma_e^2}\right) = \ln(1.26094\tau)$$

and the first and second derivative of the gamma function Γ at $x = 1$.

$$\Gamma^{(1)}(1) = -0.5772, \quad \Gamma^{(2)}(1) = 1.9781$$

The resulting thermally induced stresses are

$$\sigma_{rr} = \frac{\alpha E\Delta\vartheta}{1-\nu}\left(-\frac{1}{2\rho}+\frac{1}{2}-\ln\rho\right)I_0^{-1} - \left(\frac{1}{2}-\frac{1}{2\rho}\right),$$
$$\sigma_{\theta\theta} = \frac{\alpha E\Delta\vartheta}{1-\nu}\left(\frac{1}{2\rho}-\frac{1}{2}-\ln\rho\right)I_0^{-1} - \left(\frac{1}{2}+\frac{1}{2\rho}\right) \tag{A.2}$$

with $\rho = R/x$ and the coefficient of thermal expansion α, the Young's modulus E, the Poisson ratio ν and the temperature difference $\Delta\vartheta$ between undisturbed formation temperature ϑ_0 and temperature after cooling ϑ.

As we consider the fractures as mode I type fractures we only need to consider the effect of the tangential stress $\sigma_{\theta\theta}$ which is acting perpendicular to the already existing fracture plane. The integral of Paris and Sih (Eq. (A.1)) is then written as

$$K_I(D) = \frac{1}{\sqrt{\pi L}}D\int_{-L}^{L}\left(G + x\frac{(I_0^{-1}-1)}{2R} + I_0^{-1}\ln x\right)\left(\frac{L+x}{L-x}\right)^{1/2}dx \tag{A.3}$$

using $D = \alpha E\Delta\vartheta/1-\nu$

$$G = -\frac{1}{2}(I_0^{-1}+1) - I_0^{-1}\ln R \tag{A.4}$$

and the transformations

$$\frac{\sigma_{00}}{D} = -\frac{1}{2}(I_0^{-1}+1) + I_0^{-1}\left(\frac{1}{2\rho}-\ln\rho\right) - \frac{1}{2\rho}$$

$$\frac{\sigma_{\theta\theta}}{D} = -\frac{1}{2}(I_0^{-1}+1) + \frac{1}{2\rho}(I_0^{-1}-1) - I_0^{-1}\ln\rho$$

$$\frac{\sigma_{\theta\theta}}{D} = -\frac{1}{2}(I_0^{-1}+1) - I_0^{-1}\ln R + x\frac{(I_0^{-1}-1)}{2R} + I_0^{-1}\ln x$$

$$\frac{\sigma_{\theta\theta}}{D} = G + x\frac{(I_0^{-1}-1)}{2R} + I_0^{-1}\ln x$$

In Eq. (A.3) it is assumed that the fracture never reaches the front of the temperature perturbation, b_0. The exact limits for integration are the x-values for which $\sigma_{\theta\theta}$(therm) (Eq. (A.2)) becomes zero. Physically this means that a thermal stress is acting on the fracture planes only for values smaller than the distance between the front of the temperature perturbation and the center of the hole. Outside the temperature perturbation the thermal stress is zero. Numerically calculated values of $\ln(b_0)$ for values of t between 0 and 10000 are well fitted by the function

$$\ln(b_0) = 0.52514 + 1.0245\log(\tau)$$

Solving for b_0 leads to

$$b_0 = e^{0.52514+1.0245\log(\tau)}$$

which allows the use of $\pm b_0$ as a correct upper and lower limit for the integration. As we are interested in the case of KTB, we use $R = 0.1873$ m ($14\frac{3}{4}$ inch) as borehole radius and $\kappa = 10^{-6}$ m/s as thermal diffusivity. Using these values and a circulation (cooling) time of $T = 20$ h the front of the temperature perturbation reaches $b_0 = 2.33$, or for $T = 60$ h, $b_0 = 3.80$. For further investigation we have to keep this limitation in mind.

The integral in Eq. (A.3) can be separated in three parts:

$$K_I(D) = K_{I1} + K_{I2} + K_{I3}$$

which leads to the following three integrals having to be solved:

$$K_{I1} = \frac{1}{\sqrt{\pi L}} DG\int_{-L}^{L}\left(\frac{L+x}{L-x}\right)^{1/2} dx$$

$$K_{I2} = \frac{1}{\sqrt{\pi L}} D\frac{(I_0^{-1}-1)}{2R}\int_{-L}^{L} x\left(\frac{L+x}{L-x}\right)^{1/2} dx$$

Table 4
Fourier number τ, function I_0^{-1} and the maximum distance the temperature perturbation reaches for R equal 0.1873 m and κ equal 10^{-6} m^2/s

Time of cooling, T (h)	20	40	60
$\tau = \kappa^* T/R^2$	2.052	4.104	6.157
I_0^{-1}	0.36908	0.32120	0.29547
b_0	2.32809	3.16911	3.79562

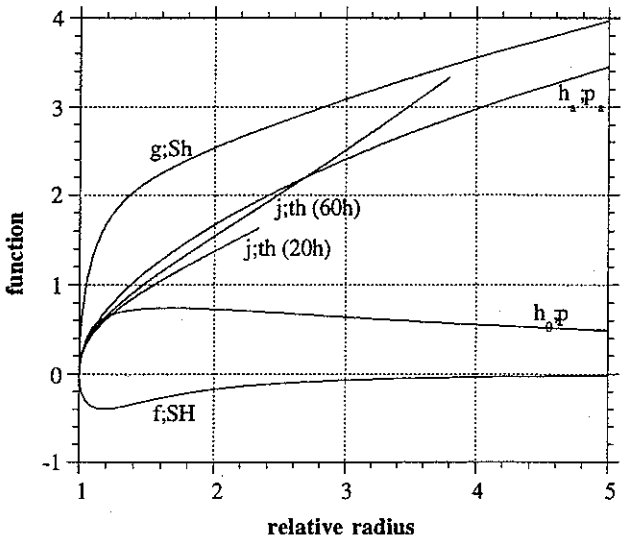

Fig. 19. Functions f, g, h_b, h_u and j for the calculation of the stress intensity factor K_I. The function j is given for two different times of cooling. The functions j are ending towards higher relative radii at b_0 which is the maximum distance the temperature disturbance reached during the time of cooling. The nomenclature of the curves means e.g. $g;S_h$, function g representing the influence of S_h.

$$K_{I3} = \frac{1}{\sqrt{\pi L}} DI_0^{-1}\int_{-L}^{L}\ln(x)\left(\frac{L+x}{L-x}\right)^{1/2} dx$$

With $b = L/R$ the results are written as

$$K_{I1} = -DG\sqrt{R}\sqrt{\pi b}\left[1 - \frac{2}{\pi}a\sin\left(\frac{1}{b}\right)\right]$$

$$K_{I2} = D\sqrt{R}(1 - I_0^{-1})\sqrt{\frac{b}{\pi}}\sqrt{b^2-1}$$

$$K_{I3} = -D\sqrt{R}I_0^{-1}\sqrt{\pi b}\ln R\frac{\ln L}{\ln R} - \frac{2}{\pi}a\sin\left(\frac{1}{b}\right)$$

$$K_{I3} = D\sqrt{RI_0^{-1}}\sqrt{\pi b}\ln R\left[\frac{2}{\pi}a\sin\left(\frac{1}{b}\right)\right] + (1$$

$$- I_0^{-1})\sqrt{\frac{b}{\pi}}\sqrt{b^2-1} - I_0^{-1}\sqrt{\pi b}\ln b$$

and finally the stress intensity factor for a thermally induced stress field is

$$K_I(D) = D\sqrt{R}j(I_0^{-1}, b)$$

with

$$j(I_0^{-1}, b) = \left(\frac{1}{2} + \frac{1}{2}I_0^{-1}\right)\sqrt{\pi b}\left[1 - \frac{2}{\pi}a\sin\left(\frac{1}{b}\right)\right] + (1$$

$$- I_0^{-1})\sqrt{\frac{b}{\pi}}\sqrt{b^2-1} - I_0^{-1}\sqrt{\pi b}\ln b$$

Typical values for the time of cooling (circulation) in

the KTB main hole are 20 to 60 h. Table 4 compiles the Fourier number τ, the value of I_0^{-1} and the maximum distance b_0 the temperature disturbance reaches from the center of the hole for these times of circulation.

The stress intensity functions j for T equal to 20 and 60 h of cooling are compared to the stress intensity functions f, g, h_0 and h_a in Fig. 19. The influence of the temperature change gets only slightly more important with increasing time of cooling. Fig. 20 displays the sum of the functions shown in Fig. 19. The upper 3 curves include the influence of the thermal stress whereas the lowest curve excludes this influence.

Using the combination of values given in Table 5 which are regarded as typical and representative for the situation at the KTB site the stress intensity factor K_I is calculated including the influence of the thermally induced stress by

$$K_I = -S_H\sqrt{R}f(b) - S_h\sqrt{R}g(b) + p_b\sqrt{R}h_b(b) + p_a\sqrt{R}h_a(b) + D\sqrt{R}j(b) \quad (A.5)$$

D is the thermal stress directly at the borehole wall given by Eq. (A.4).

The pressure p_a in the fracture is assumed to decrease reciprocal. The stress intensity factor K_I is calculated for all combinations of the mud pressure and amount of cooling contained in the intervals given above for relative radii between 1 and 3. To get an overview on the results and on the influence of the variables pressure and temperature difference, K_I is plotted as function of pressure and relative radius or

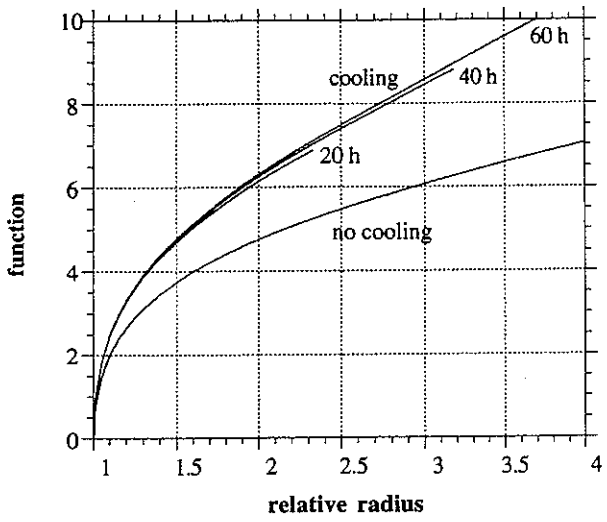

Fig. 20. Displayed are the sum of the functions f, g, h_b, h_a and j for no cooling, 20 h, 40 h and 60 h cooling.

Table 5
Representative values at the KTB site used for the calculation of the stress intensity factor K_I

S_H	180 MPa
S_h	80 MPa
R	0.15558 m
ν	0.25
κ	10^{-6} m^2/s
α	0.6×10^{-5}
T	60 h
$\Delta\vartheta$	40–80°
p_0	50–80 MPa

as function of temperature difference and relative radius with the third variable kept at a constant value.

As fractures form for positive values of the stress intensity factor which are greater than the critical stress intensity factor K_{Ic}, in the following figures only positive values of the stress intensity factor are plotted. Negative values are set to zero to improve the resolution of the figures and to pronounce combinations of pressure and cooling values which allow growth of fractures. Fig. 21(a) and (b) display the stress intensity factor for a fixed mud pressure p_b of 56 and 62 MPa as a function of the relative radius and of the temperature difference between undisturbed formation temperature and temperature of the drilling mud. All figures show a steep increase of K_I for small relative radii up to about 1.1. This steep increase of K_I indicates that small natural micro-fractures in the mm-range can act as starting points for the initiation of drilling-induced tensile fractures under the assumed stress state and borehole conditions. Even for relative radii smaller than 1.03 (corresponding to 0.5 cm in a 37.5 cm diameter borehole) the stress intensity factor is greater than common values of K_{Ic}.

The decrease of K_I for higher normalized radii is strongly dependent on the mud pressure and the temperature difference. For low pressure and low temperature differences the decrease of K_I with relative radius is rapid and steep. The influence of the pressure is dominant and leads for high pressure to positive K_I values also for great relative radius and for small temperature differences. Also the temperature difference can have significant influence on the growth of fractures, as can be seen in Fig. 21(a) and (b). At constant pressure the amount of cooling controls the relative radius at which the stress intensity factor is positive, meaning it controls the maximum extent a fracture can grow away from the borehole wall.

The stress intensity factor as a function of the relative radius and the pressure at constant temperature differences (40 K, 56 K) is shown in Fig. 22(a) and (b).

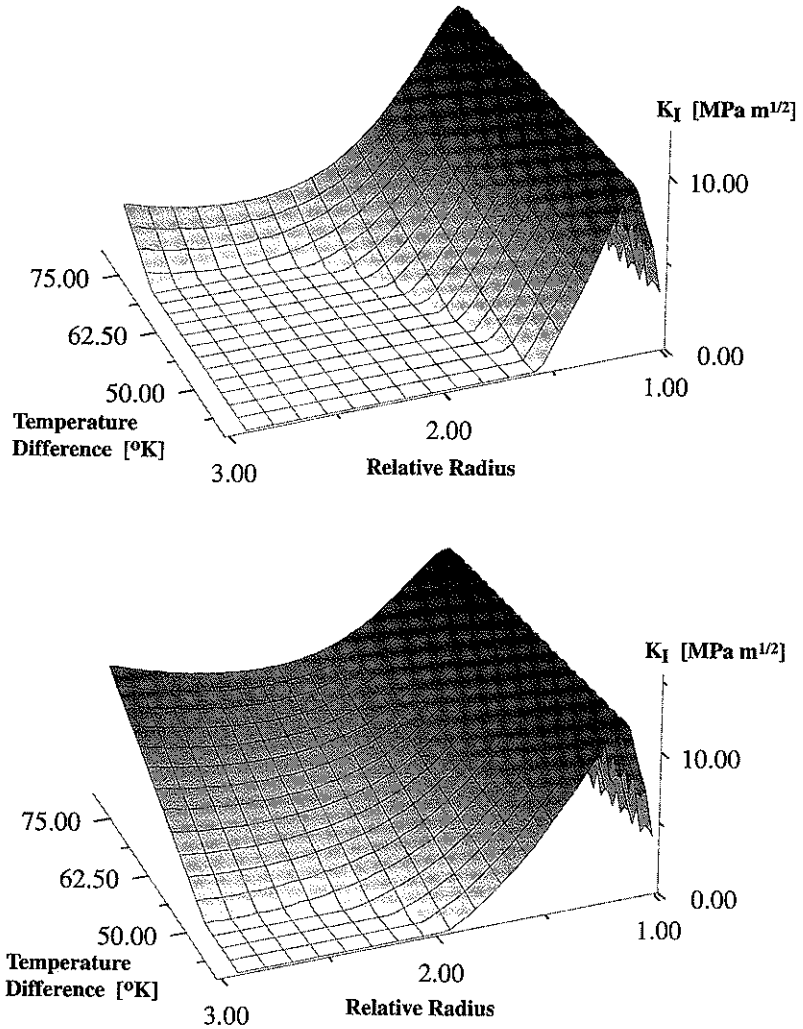

Fig. 21. The stress intensity factor K_I for a fixed mud pressure p of (a) 56 MPa and (b) 62 MPa is displayed as a function of the relative radius and of the temperature difference between undisturbed formation temperature and temperature of the drilling mud. All figures show a steep increase of K_I for small relative radii up to about 1.1.

Again for low pressure and low temperature difference the positive values of K_I are restricted to small relative radii between 1.4 and 2.0. For high pressures and temperature differences the fractures can reach length greater than the relative radius 3. For such conditions the fractures could truly leave the area close to the borehole wall and the chance to connect to natural fractures becomes relevant. If a fracture connects to the natural fracture systems which is either over- or underpressured with respect to the borehole this should be observable in temperature logs and in chemical analysis of the mud for trip gases and influx of pore fluid. As such indications for influx to the wellbore are only found in areas where major fractures cross-cut the well a connection of the drilling-induced fractures to the natural fracture system seems to be unlikely. This also means that the fractures should be restricted to the area close to the borehole. If they are truly restricted to small radii it is not possible that the total amount of thermally induced stress and stress due to the mud pressure acted at the same time on the rock, because these stress conditions would allow the fracture to propagate further than 3 radii away from the borehole. It is also quite unlikely that both act at the same time as commonly the highest pumping pressures are encountered when the pumps are started at the begin of drilling, whereas the influence of cooling gets more important with time of drilling and circulation. Thus, it should be highest at the end of a drilling period.

Finally, to study the influence of the time of cooling all the K_I values are computed for $T = 20$ h and $T = 40$ h. It is found that the influence of the cooling time is minor compared to the influences of the other variables. Only a slight decrease of the stress intensity factor K_I for decreasing times of cooling is observed.

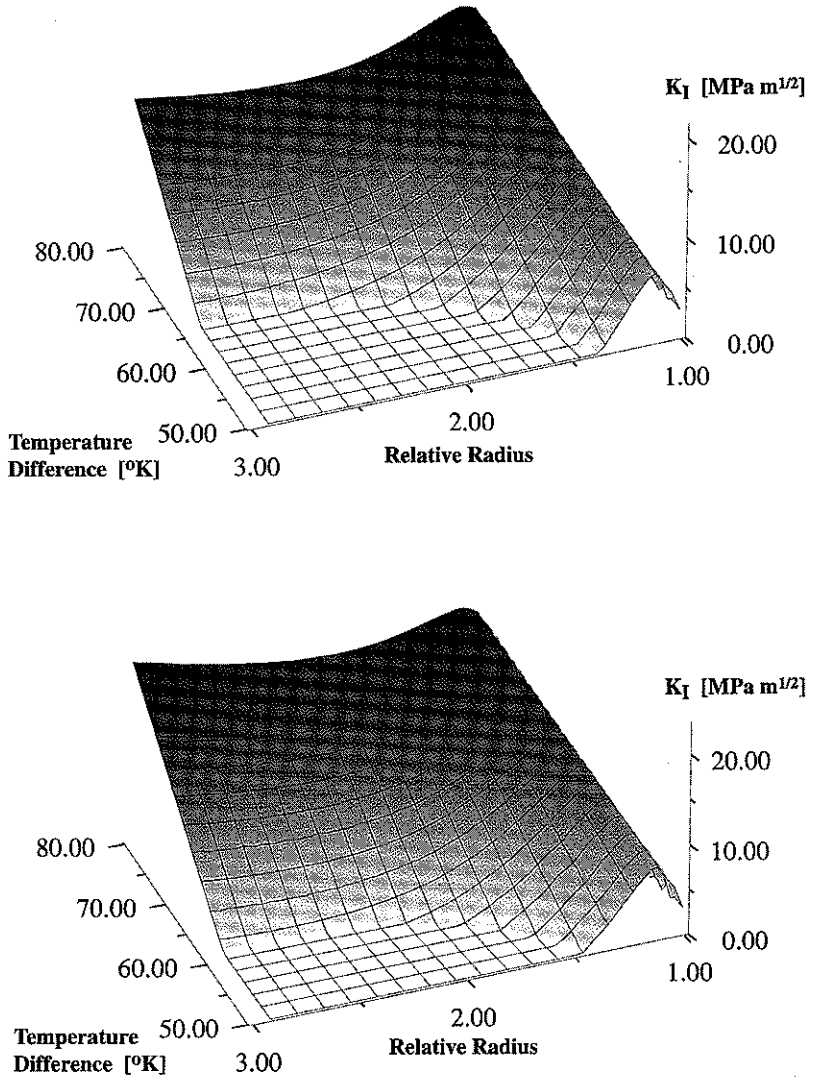

Fig. 22. The stress intensity factor K_I is shown as a function of the relative radius and the pressure at a constant temperature difference of (a) 40 K and (b) 56 K. For low pressure and low temperature difference the positive values of K_I are restricted to small relative radii between 1.4 and 2.0. For high pressures and temperature differences the fractures can reach length greater than the relative radius 3.

References

[1] Bell JS, Gough DI. The use of borehole breakouts in the study of crustal stress. In Zoback MD, Haimson BC, editors. Hydraulic fracturing stress measurements. Washington, DC: National Academy Press, 1983. p. 201–9.

[2] Zoback MD, Moos D, Mastin L. Wellbore breakouts and in situ stress. J. Geophys. Res. 1985;90:5523–30.

[3] Stock JM, Healy JH, Hickman SH, Zoback MD. Hydraulic fracturing stress measurements at Yucca Mountain, Nevada, and relationship to the regional stress field. J. Geophys. Res. 1985;90:8691–706.

[4] Moos D, Morin RH. Observations of wellbore failure in the Toa Baja well: implications for the state of stress in the North Coast tertiary basin, Puerto Rico. Geophys. Res. Lett. 1991;18:505–8.

[5] Zemanek J, Glenn EE, Norton LJ, Caldwell RL. Formation evaluation by inspection with the borehole televiewer. Geophysics 1970;35:254–69.

[6] Ekstrom MP, Dahan CA, Chen MY, Lloyd PM, Rossi DJ. Formation imaging with microelectrical scanning arrays. Log Anal. 1987;28:294–306.

[7] Hubbert MK, Willis DG. Mechanics of hydraulic fracturing. Petr. Trans. AIME. 1957;210:153–63.

[8] Haimson B, Fairhurst C. Initiation and extension of hydraulic fractures in rocks. Soc. Petr. Eng. J. 1967;September:310–8.

[9] Emmermann R, Wohlenberg J, editors. The German continental deep drilling program. Springer Verlag, 1989.

[10] Hirschmann G. On the geological interpretation of the 3D seismic data with special regard to the information from the KTB boreholes. In: Dürbaum H-J, Reichert C, Sadowiak P, Bram K, editors. KTB Report 92-5. Hannover: NLfB-KTB, 1992. p. 351–73.

[11] Wenzel F, Bram K, Reichert Ch. Calibration of a crustal reflector at the KTB site, Annales Geophysicae, Supplement 1 to Vol. 13, Part I: Solid Earth Geophysics and Natural Hazards, 1995.

[12] Draxler J, Heinschild H-J, Hirschmann G, Kessels W, Kohl J, Wöhrl T. Klufterkennung durch Bohrlochmessungen,

Gasanalyse und Kernaufnahme. In: Emmermann R, Giese P, editors. KTB-Report 90-4. 1990.

[13] Hirschmann G. KTB Hauptbohrung: what's beneath the seismic reflector SE1? In: Emmermann R, Lauterjung J, Umsonst T, editors. KTB-Report 93-2, Hannover, 1993. p. 141–4.

[14] de Wall H, Duyster J, Hirschmann G, Kontny A, Lich S, Spangenberg E. Die Störungszone in 7 km Tiefe: Ursachen eines seismischen Reflektors. KTB Report 94-4. 1995.

[15] Kappelmeyer O, Gerard A, Schloemer W, Ferrandes R, Rummel F, Benderitter Y. European HDR project at Soultz-sous-Forêts: general presentation. In: Bresee JC, editor. Geothermal energy in Europe. Gordon and Breach Science Publishers, 1992. p. XVII–XLIII.

[16] Huber K. Aufbereitung und Darstellung elektrischer Abbilder der Bohrlochwand an Beispielen aus der KTB: Vorbohrung. Diploma thesis, Karlsruhe, 1991.

[17] Brudy M, Zoback MD. Compressive and tensile failure of boreholes arbitrarily inclined to principal stress axis: application to the KTB boreholes. 34th US Symposium on Rock Mechanics. Germany, 1993.

[18] Borm G, Lempp C, Natau O, Röckel T. Instabilities of borehole and drillcores in crystalline rocks, with examples from the KTB pilot hole. Sci. Drill. 1989;1:105–14.

[19] Brudy M, Fuchs K, Zoback MD. Stress orientation profile to 6 km depth in the KTB main borehole. In: Bram K, Draxler JK, editors. KTB Report 93-1. Hannover: NLfB-KTB, 1993. p. 281–300.

[20] Tenzer H, Mastin L, Heinemann B. Determination of planar discontinuities and borehole geometry in the crystalline rock of borehole GPK1 at Soultz-sous-Forêts. In: Bresee, editor. Geothermal science and technology. Gordon and Breach Publishers, 1992. p. 31–68.

[21] Nagel R. Das Spannungsfeld in der Geothermiebohrung Soultz-sous-Forêts abgeleitet aus vertikalen Strukturen in einer Tiefe von 1.9 bis 3.6 km. Diploma thesis, Universität Karlsruhe, 1994.

[22] Röckel T, Natau O, Dietrich H-G. Core reorientation by comparison of core instabilities and borehole instabilities. In: Emmermann R, Dietrich H-G, Lauterjung J, Wöhrl T, editors. KTB Report 92-2. Hannover: NLfB-KTB, 1992. p. F1–F7.

[23] Baumgärtner J, Rummel F, Zoback MD. Hydraulic fracturing in situ stress measurements to 3 km depth in the KTB pilot hole VB. In: Bram K, Draxler JK, Kessels W, Zoth G, editors. KTB Report 90-6a. Hannover: NLfB-KTB, 1990. p. 353–99.

[24] Brudy M, Fuchs K, Zoback MD. Tectonic stresses: a profile down to the mid-crust. In: Emmermann R, Giese P, Lauterjung J, Umsonst T, editors. KTB-Report 94-2. Hannover: NLfB-KTB, 1994. p. A107–16.

[25] Mastin LG, Heinemann B, Krammer A, Fuchs K, Zoback MD. Stress orientation in the KTB pilot hole determined from wellbore breakouts. Sci. Drill. 1991;2:1–12.

[26] Barton C, Zoback MD. Stress perturbations associated with active faults penetrated by boreholes: possible evidence for near-complete stress drop and a new technique for stress magnitude measurement. J. Geophys. Res. 1994;99:9373–90.

[27] Hiramatsu Y, Oka Y. Determination of the stress in rock unaffected by boreholes or drifts, from measured strains or deformations. Int. J. Rock Mech. Min. Sci. 1968;5:337–53.

[28] Fairhurst C. Methods of determining in situ rock stresses at great depth. Report TRI-68. Missouri River Div. Corps of Engineers, 1968.

[29] Zoback MD, Apel R, Baumgärtner J, Brudy M, Emmermann R, Engeser B, Kessels W, Fuchs K, Rischmüller H, Rummel F, Vernik L. Upper-crustal strength inferred from stress measurements to 6 km depth in the KTB borehole. Nature 1993;365:633–5.

[30] Ahorner L. Present-day stress field and seismotectonic block movements along major fault zones in western Europe. Tectonophysics 1975;29:233–49.

[31] Illies H, Greiner G. Regionales stress Feld und Neotektonik in Mitteleuropa. Oberrh. Geol. Abh. 1976;25:1–40.

[32] Larroque JM, Laurent P. Evolution of the stress field pattern in the south of the Rhine Graben from Eocene to the present. Tectonophysics 1988;148:41–58.

[33] Shamir G, Zoback MD. Stress orientation profile to 3.5 km depth near the San Andreas Fault at Cajon Pass, California. J. Geophys. Res. 1992;97:5059–80.

[34] Hickman S, Moos D, Barton C, Khakaev B. In-situ stress and borehole breakouts in the Tyrnauz well, Caucasus Mountains, USSR (abs). AGU Fall Meeting. EOS Trans, 1991. p. 511.

[35] Peska P, Zoback MD. Compressive and tensile failure of inclined wellbores and determination of in situ stress and rock strength. J Geophys Res 1995, submitted for publication.

[36] Kirsch G. Die Theorie der Elastizität und die Bedürfnisse der Festigkeitslehre. Z. Ver. Ingen. 1898;42:797–807.

[37] Moos D, Zoback MD. Utilization of observations of well bore failure to constrain the orientation and magnitude of crustal stresses: application to continental, deep sea drilling project, and ocean drilling program boreholes. J. Geophys. Res. 1990;95:9305–25.

[38] Nur A, Byerlee JD. An exact effective sress law for elastic deformation of rock with fluids. J Geophys Res 1971:6414–9.

[39] Schmitt DR, Zoback MD. Diminished pore pressure in low-porosity crystalline rock under tensional failure: apparent strengthening by dilatancy. J. Geophys. Res. 1992;97:273–88.

[40] Engeser B. Auswahl eines Spülungssystems für die speziellen Anforderungen des KTB-Projektes. In: Emmermann R, Giese P, editors. KTB Report 88-10. Hannover: NLfB-KTB, 1988. p. 231–44.

[41] Ritchie RH, Sakakura AY. Asymptotic expansions of solutions of the heat conduction equation in internally bounded cylindrical geometry. J. Appl. Phys. 1956;27:1453–9.

[42] Nowacki W. Thermoelasticity. Reading, MA: Addison-Wesley, 1962.

[43] Stephens G, Voight B. Hydraulic fracturing theory for conditions of thermal stress. Int. J. Rock Mech. Min. Sci. 1982;19:279–84.

[44] Skinner BJ. Thermal expansion. In: Handbook of physical constants. The Geological Society of America, 1966. p. 76–96.

[45] Zoth G. Temperature measurements during the 6000 m logging campaign in the KTB-Oberpfalz HB. In: Bram K, Draxler JK, editors. KTB Report 93-1. Hannover: NLfB-KTB, 1993. p. 215–7.

[46] Röckel T, Natau O. Tiefbohrung KTB Oberpfalz VB - erste Ergebnisse felsmechanischer Indexversuche bis 1998 m. In: Emmermann R, Dietrich H-G, Heinisch M, Wöhrl T, editors. KTB Report 89-2. Hannover: NLfB-KTB, 1989. p. H1–H22.

[47] Röckel T, Natau O. Rock mechanics, depth interval 0–6000 m. In: Emmermann R, Dietrich H-G, Lauterjung J, Wöhrl T, editors. KTB Report 92-2. Hannover: NLfB-KTB, 1992. p. E1–E7.

[48] Rummel F, Baumgärtner J. Hydraulic fracturing stress measurements in the GPK1 borehole, Soultz-sous-Forêts. In: Bresee J, editor. Geothermal energy in Europe. 1992. p. 119–37.

[49] Engeser B, Huenges E, Kessels W, Kück J, Wohlgemuth L. The 6000 m hydrofrac test in the KTB main borehole: design, implementation and preliminary results. In: Bram K, Draxler JK, editors. KTB Report 93-1. Hannover: NLfB-KTB, 1993. p. 301–36.

[50] Sonnleitner M. Vergleich unterschiedlicher Methoden der Spannungsinversion von Erdbebendaten: am Beispiel von Erdbeben aus der Region Vogtland/westl, Böhmen. Diploma thesis, Ludwig-Maximilians-Universität München, 1993.

[51] Winter R-B. Bruchmechanische Gesteinsuntersuchungen mit dem Bezug zu hydraulischen Frac-Versuchen in Tiefbohrungen. Ph.D. thesis, Ruhr-Universität Bochum, 1983.
[52] Rummel F, Winter RB. Fracture mechanics as applied to hydraulic fracturing stress measurements. Earthq. Predict. Res. 1983;2:33–45.
[53] Müller W, Rummel F. Fracture toughness of granites. Geol Jahrbuch E 1987:125–36.
[54] Rummel F, Thieme B. Bestimmung bruchmechanischer Kenngrößen am Kernmaterial der Vorbohrung des Kontinentalen Tiefbohrprojektes der Bundesrepublik Deutschland. Report Ruhr-Universität Bochum, Inst. Geophysik, 1991.
[55] Paris PC, Sih GC. Stress analysis of cracks. In: Fracture Toughness Testing and its Applications. American Society for Testing and Materials, 1965. p. 30–83.
[56] Rummel F. Fracture mechanics approach to hydraulic fracturing stress measurements. In: Atkinson BK, editor. Fracture mechanics of rock. London: Academic Press, 1987. p. 217–40.
[57] Spencer LV, Fano U. Energy spectrum resulting from electron slowing down. Phys. Rev. 1954;93:1172–81.